NASA/TM-2000-210289

Parametric Weight Comparison of Advanced Metallic, Ceramic Tile, and Ceramic Blanket Thermal Protection Systems

David E. Myers, Carl J. Martin, and Max L. Blosser
Langley Research Center, Hampton, Virginia

June 2000

The NASA STI Program Office ... in Profile

Since its founding, NASA has been dedicated to the advancement of aeronautics and space science. The NASA Scientific and Technical Information (STI) Program Office plays a key part in helping NASA maintain this important role.

The NASA STI Program Office is operated by Langley Research Center, the lead center for NASA's scientific and technical information. The NASA STI Program Office provides access to the NASA STI Database, the largest collection of aeronautical and space science STI in the world. The Program Office is also NASA's institutional mechanism for disseminating the results of its research and development activities. These results are published by NASA in the NASA STI Report Series, which includes the following report types:

- TECHNICAL PUBLICATION. Reports of completed research or a major significant phase of research that present the results of NASA programs and include extensive data or theoretical analysis. Includes compilations of significant scientific and technical data and information deemed to be of continuing reference value. NASA counterpart of peer-reviewed formal professional papers, but having less stringent limitations on manuscript length and extent of graphic presentations.

- TECHNICAL MEMORANDUM. Scientific and technical findings that are preliminary or of specialized interest, e.g., quick release reports, working papers, and bibliographies that contain minimal annotation. Does not contain extensive analysis.

- CONTRACTOR REPORT. Scientific and technical findings by NASA-sponsored contractors and grantees.

- CONFERENCE PUBLICATION. Collected papers from scientific and technical conferences, symposia, seminars, or other meetings sponsored or co-sponsored by NASA.

- SPECIAL PUBLICATION. Scientific, technical, or historical information from NASA programs, projects, and missions, often concerned with subjects having substantial public interest.

- TECHNICAL TRANSLATION. English-language translations of foreign scientific and technical material pertinent to NASA's mission.

Specialized services that complement the STI Program Office's diverse offerings include creating custom thesauri, building customized databases, organizing and publishing research results ... even providing videos.

For more information about the NASA STI Program Office, see the following:

- Access the NASA STI Program Home Page at ***http://www.sti.nasa.gov***

- E-mail your question via the Internet to help@sti.nasa.gov

- Fax your question to the NASA STI Help Desk at (301) 621-0134

- Phone the NASA STI Help Desk at (301) 621-0390

- Write to:
  NASA STI Help Desk
  NASA Center for AeroSpace Information
  7121 Standard Drive
  Hanover, MD 21076-1320

NASA/TM-2000-210289

Parametric Weight Comparison of Advanced Metallic, Ceramic Tile, and Ceramic Blanket Thermal Protection Systems

David E. Myers, Carl J. Martin, and Max L. Blosser
Langley Research Center, Hampton, Virginia

National Aeronautics and
Space Administration

Langley Research Center
Hampton, Virginia 23681-2199

June 2000

The use of trademarks or names of manufacturers in the report is for accurate reporting and does not constitute an official endorsement, either expressed or implied, of such products or manufacturers by the National Aeronautics and Space Administration.

Available from:

NASA Center for AeroSpace Information (CASI)
7121 Standard Drive
Hanover, MD 21076-1320
(301) 621-0390

National Technical Information Service (NTIS)
5285 Port Royal Road
Springfield, VA 22161-2171
(703) 605-6000

ABSTRACT

A parametric weight assessment of advanced metallic panel, ceramic blanket, and ceramic tile thermal protection systems (TPS) was conducted using an implicit, one-dimensional (1-D) finite element sizing code. This sizing code contained models to account for coatings, fasteners, adhesives, and strain isolation pads. Atmospheric entry heating profiles for two vehicles, the Access to Space (ATS) vehicle and a proposed Reusable Launch Vehicle (RLV), were used to ensure that the trends were not unique to a certain trajectory. Ten TPS concepts were compared for a range of applied heat loads and substructural heat capacities to identify general trends. This study found the blanket TPS concepts have the lightest weights over the majority of their applicable ranges, and current technology ceramic tiles and metallic TPS concepts have similar weights. A proposed, state-of-the-art metallic system which uses a higher temperature alloy and efficient multilayer insulation was predicted to be significantly lighter than the ceramic tile systems and approaches blanket TPS weights for higher integrated heat loads.

SYMBOL LIST

C_p	Total Structural Heat Capacity, Btu/ft^2-°R
c_p	Specific Heat Capacity, Btu/lb-°R
k	Thermal Conductivity, Btu/ft-s-°R
P	Pressure, lb/ft^2
Q	Total Unit Heat Load, Btu/ft^2
q	Heat Flux, Btu/ft^2-s
T	Temperature, °R
T_{Rad}	Radiation Equilibrium Temperature, °F
t	Structural or Insulation Thickness, in. or ft.
tx1	Inner Insulation on a TPS Concept, in.
tx2	Outer Insulation on a TPS Concept, in.
ε	Emissivity
ρ	Structural Density, lb/ft^3

INTRODUCTION

A number of reusable hypersonic vehicles are being proposed and studied to augment the current Space Shuttle. Proposed vehicles include the Reusable Launch Vehicle (RLV)[1], military spaceplane[2], spaceplanes for tourism[3], space trucks[4], suborbital package delivery vehicles[5], and hypersonic airbreathing vehicles[6]. One of the key technologies required by all of these vehicles is a reusable, low maintenance, light weight thermal protection system (TPS). Although the primary function of a TPS is to protect the vehicle from aerodynamic heating, the operational capability and system weight also have significant impact on vehicle performance. For commercial viability, the TPS must minimize

life cycle costs to enable delivery of commercial payloads at reasonable cost. For military applications, the TPS must enable high performance, rapid response, and rapid turnaround under adverse conditions.

The most extensive experience with reusable TPS is with the ceramic tile and blanket TPS on the Space Shuttle orbiter. Although the orbiter TPS does an excellent job of protecting the vehicle from aerodynamic heating, more than 40,000 work hours[7] are expended to refurbish the TPS between flights. Because of the fragile nature of the orbiter current TPS, the orbiter cannot fly through rain, and great care must be taken in routine maintenance to avoid damaging the TPS. Such fragile, high maintenance TPS is clearly unacceptable for future commercial and rapid turnaround hypersonic vehicles.

To achieve the goals of low life cycle cost and rapid turnaround, TPS for future reusable vehicles must be robust and low maintenance, yet efficiently protect the vehicles from aerodynamic heating. The TPS must survive the operational environment with minimal refurbishment. That environment includes low- and high-velocity impact (e.g. dropped tools during maintenance procedures and orbital debris, respectively); rain; and aerothermal, acoustic, and thermal-mechanical loads. In addition, the TPS should be easy to inspect, maintain, and repair; should not require waterproofing between flights; and should be rugged and damage tolerant. Of course, an overriding concern for any TPS is system weight. TPS weight is particularly important for single-stage-to-orbit vehicles which have large surface areas requiring thermal protection. There is generally a tradeoff between TPS durability and weight.

A variety of reusable TPS concepts are being developed to address the requirements of future hypersonic vehicles. Development of improved ceramic TPS is being led by the NASA Ames Research Center[8]. Ceramic tiles, such as alumina enhanced thermal barrier (AETB)[9] with toughened unipiece fibrous insulation (TUFI) and reaction cured glass (RCG) coatings, have been developed to be significantly stronger and more resistant to rain erosion than the current Shuttle tiles. Tailorable advanced blanket insulation (TABI)[10], also developed by NASA Ames, is being proposed as a cheaper more easily integrated and installed replacement for tiles over large areas of future vehicles. Metallic TPS represent another promising alternative reusable concept. Much of the development of metallic TPS[11] is being led by the NASA Langley Research Center (LaRC). Concepts development proceeded from early stand-off heat shields to titanium multiwall concepts (TIMW)[12] to prepackaged superalloy honeycomb sandwich panels (SA/HC)[13]. The detailed design and fabrication of the TIMW and SA/HC TPS concepts were performed by Rohr Incorporated (now B. F. Goodrich Aerospace). The SA/HC TPS was further improved and tested under a recent cooperative agreement[11] between McDonnell Douglas Aerospace and the NASA LaRC. A derivative of the SA/HC concept, developed by B. F. Goodrich, is the primary TPS on the X-33[1], an experimental RLV technology demonstrator vehicle (Appendix A).

Selection of the optimum TPS for a particular vehicle is a complex and challenging task that requires consideration of not only weight, but also operability, maintenance, durability, initial cost, life-cycle cost, and integration with the vehicle structures, including cryogenic propellant tanks. The current paper undertakes a much less ambitious task: weight comparisons among several TPS concepts using a one-dimensional, transient TPS sizing code. No structural resizing is performed in the current study. Component dimensions from existing designs are used. Three families of TPS are considered: metallic panels, rigid ceramic tiles, and flexible ceramic blankets. This includes current Shuttle TPS, advanced TPS which have been fabricated and tested, and proposed TPS concepts which incorporate improved materials and designs. For this study, the TPS is assumed to be directly attached to a smooth, adiabatic structure and is sized using entry heating profiles representative of future reusable reentry vehicles. The material properties and assumptions used in the analysis are documented in this paper. Key parameters, such as total heat load and structural heat capacity, are varied to obtain TPS weight comparisons over a wide range of conditions.

ANALYSIS

This section describes the basic assumptions and analytical methods used in the parametric study of TPS weights. Included are details of the simplified thermal problem analyzed, the one-dimensional TPS sizing code used, and model verification studies performed. Further details are included in the appendices. Appendix B includes the comparisons of the 1-D analysis model results with 2-D detailed model results for all the TPS concepts, Appendix C includes the material properties used in the thermal models, and Appendix D includes the component weight models for the TPS concepts.

Simplified Thermal Model

The idealized TPS and structure combination considered in this study is shown in figure 1. This simplified arrangement was selected so that the performance of the various thermal protection systems could be directly compared. The TPS is directly attached to an underlying 0.1 inch-thick aluminum structure. A transient heat flux profile is applied to the outer surface of the TPS, and the inner surface of the structure is assumed to be adiabatic, or perfectly insulated. The structure is limited to a maximum temperature of 300 ºF, and the minimum required thermal protection system thickness, t, is determined, or sized, to satisfy this temperature limit.

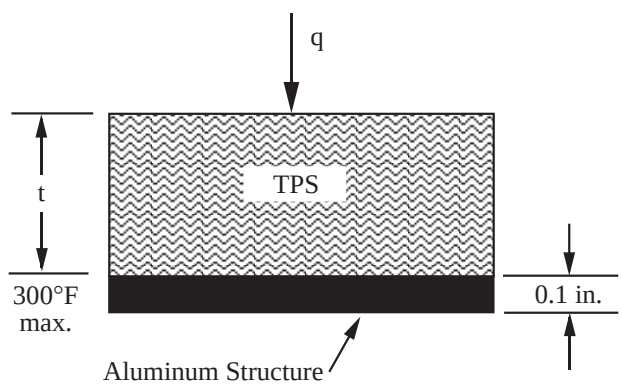

Figure 1. Simplified thermal model of TPS sizing problem.

One-dimensional (1-D) TPS Sizing Code

A thermal protection system sizing code was used to determine the required TPS thickness and resulting weight. The TPS sizing code uses a nonlinear, implicit, one-dimensional, transient, finite element solution technique to compute temperatures throughout the thermal protection system. The code includes thermal and mass models of each TPS concept that account for coatings, adhesives, fasteners, and strain isolation pads. A schematic of the thermal model for TABI is shown in figure 2 as an example. Further details concerning the models used for each TPS concept are contained in a following section, and the weight models are listed in Appendix D. In the transient thermal analysis, thermal properties, which may be a function of temperature and pressure, are updated at each analysis time step, and radiation to space is assumed at the surface node. After nodal temperatures are computed, the TPS is resized, and the analysis and resizing are repeated until the temperature of the structure converges to within 2 °F of the temperature limit. For TPS concepts using two insulations, such as the original super alloy honeycomb metallic TPS, an additional insulation temperature constraint is added. In general, convergence is achieved in less than six analysis and resizing cycles. Upon convergence, the final TPS insulation thickness and total weight are reported.

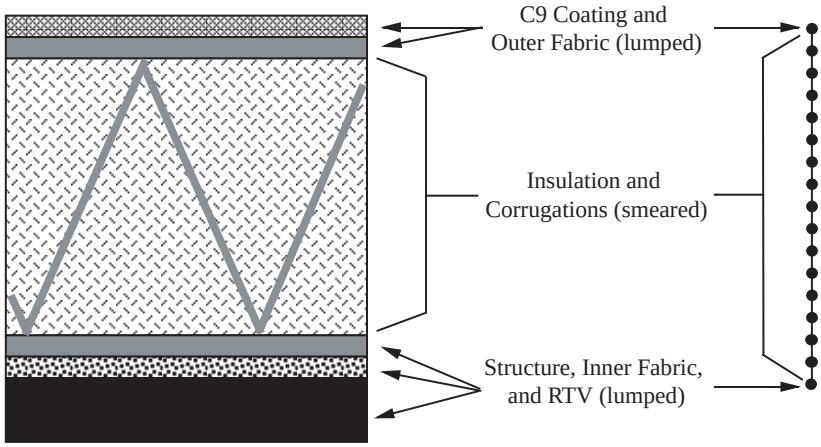

Figure 2. Conversion of a TPS concept to its thermal model

Two-dimensional (2-D) Finite Element Analysis and Comparison with 1-D Results

The TPS sizing code predicts the overall TPS thermal performance using simple, one-dimensional models. The validity of the simplifications used in the 1-D thermal analysis models was investigated by comparing the results with those from more elaborate 2-D Engineering Analysis Language (EAL)[14] finite element analyses. The 2-D models used the same material properties as the 1-D models, but included more geometric detail. For verification purposes, each TPS concept was sized using the 1-D sizing code which also predicted temperatures through the TPS and structure. A 2-D model was then constructed and analyzed using the same TPS and structural thicknesses. The temperatures, particularly the structure temperature which drives the TPS sizing, were compared to check the accuracy of the 1-D models.

In general, the metallic TPS concepts were the most difficult to reduce to one dimension. The 2-D model used varying element thicknesses to simulate a "pie wedge" of the TPS panel (Fig. 3). The Advanced Metallic Honeycomb (AMHC) concept is shown in figure 3, and the corresponding 2-D finite element model is shown in figure 4. The AMHC TPS was sized using the 1-D code and the heating profile that is shown in figure 5. This heating profile will be described in greater detail later in the paper. The required insulation thickness was computed to be 3.315 inches for the 0.1 inch aluminum structure, and these dimensions were used to create the 2-D model.

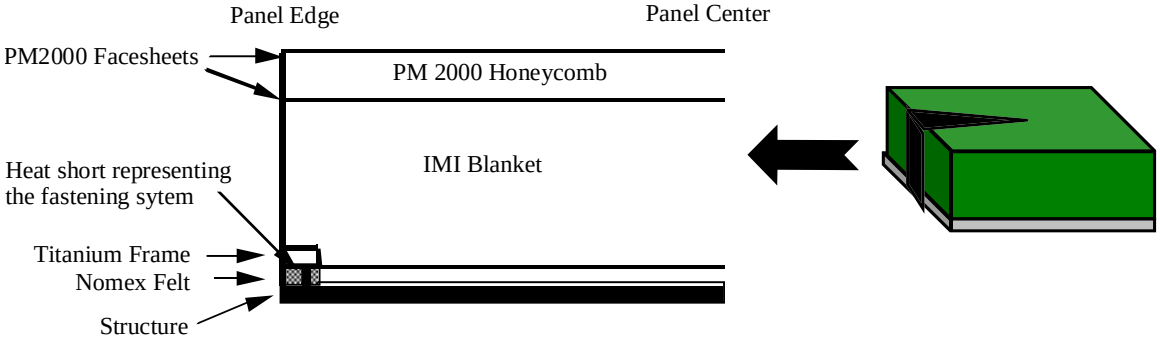

Figure 3. Two dimensional representation of the AMHC concept.

Temperatures at key locations for the one and two-dimensional models are plotted in figure 6. Center and edge temperatures are plotted for the 2-D model to illustrate the two-dimensional nature of the problem. The critical temperature profiles on this figure are those at the structure because they drive the TPS thickness. The difference between the maximum structural temperatures calculated using the two analysis models for AMHC is 4.9 °F. This model had the largest deviation between the 1-D and 2-D analyses. The second generation superalloy honeycomb concept (SA/HC2), which is similar to AMHC, had a difference of 4.5 °F. For all the other models, the structural temperatures calculated using the 1-D sizing code differed by no more than 2 °F from those calculated using the 2-D analysis. Figures comparing the temperature profiles for the other models are included in Appendix B (Figs. 31-40). Based upon these and other analyses, it was concluded that the one-dimensional sizing models were of sufficient quality for these preliminary concept comparisons.

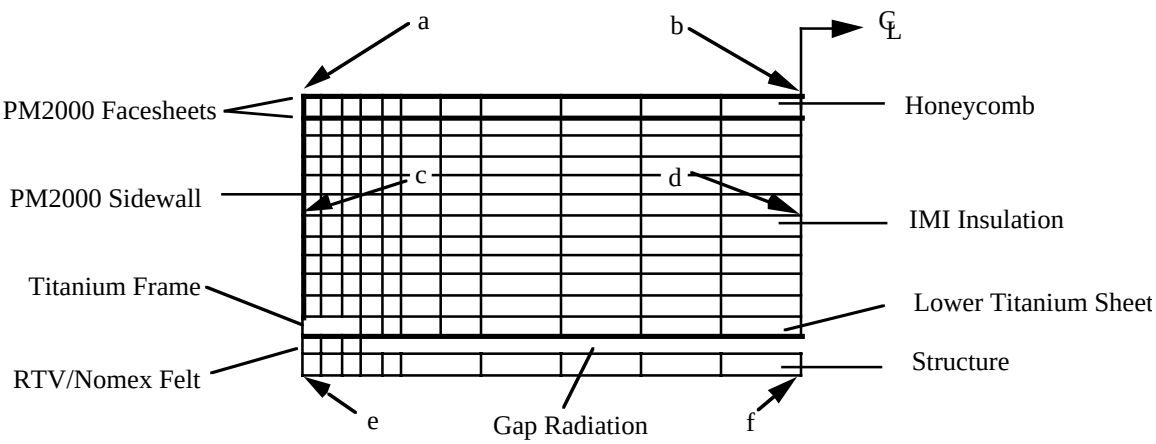

Figure 4. Two-dimensional finite element model of the AMHC concept.

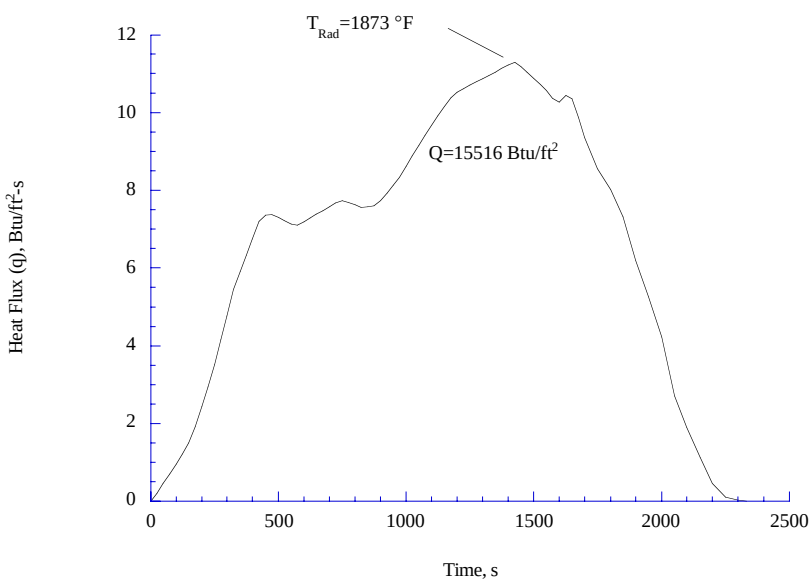

Figure 5. Heat flux profile used to verify the 1-D AMHC thermal model.

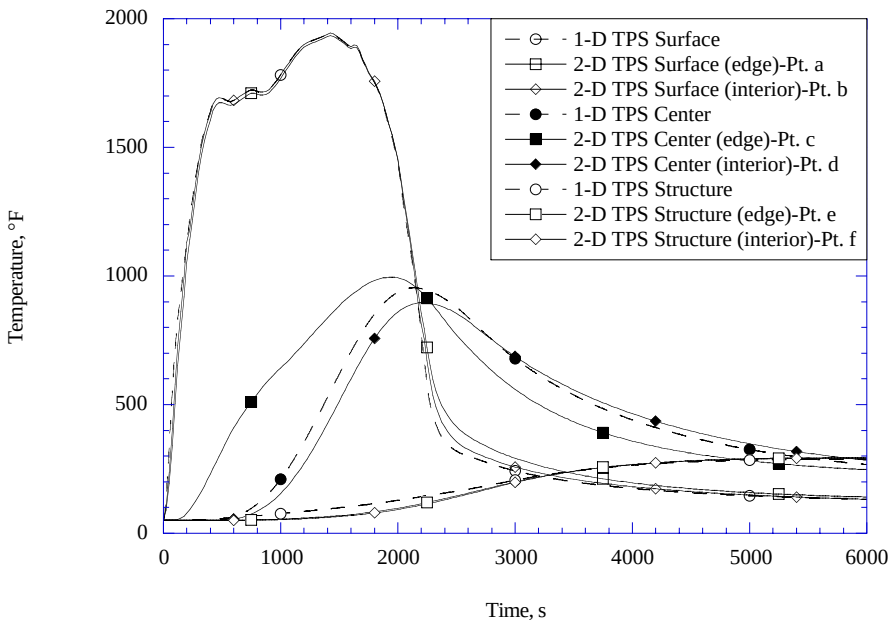

Figure 6. Transient thermal analysis results for the 1-D and 2-D AMHC thermal models.

THERMAL PROTECTION SYSTEM CONCEPTS

The one-dimensional TPS sizing code contains thermal and weight models for each TPS analyzed. A description of each TPS concept and the assumptions and properties used in the analysis are given in this section.

Flexible Ceramic Blankets

Blanket TPS consist of fibrous insulation between outer layers of woven ceramic fabric. The outer fabric layer is coated to stiffen and toughen it, and the blankets are attached to the structure with a layer of room temperature vulcanizing (RTV) adhesive. Blankets have relatively low initial costs, and their flexibility eases installation. The Advanced Flexible Reusable Surface Insulation (AFRSI) blankets used on the Space Shuttle orbiter must be waterproofed after each flight adding considerable maintenance time and expense. Blankets are initially flexible, but the addition of the C-9 coating[15] and exposure to high temperatures make the outer fabric brittle and susceptible to damage. The quilted fabric construction of AFRSI results in a rough exterior surface which promotes turbulence and thus increases aerodynamic heating and drag. The TABI TPS has a smoother surface and an increased temperature capability compared to AFRSI[10], but TABI also has waterproofing and surface brittleness issues similar to AFRSI. Testing is in progress to evaluate the durability of TABI for use on the windward side of a vehicle, and the concept's scalability to large thicknesses (3-4 inches) needs to be demonstrated. The relatively low emissivities at high temperatures of the blanket fabrics with the C-9 coating limit the heating levels where blanket TPS may be used, but higher emissivity coatings are under development[10].

Advanced Flexible Reusable Surface Insulation

Advanced Flexible Reusable Surface Insulation was developed as a partial replacement for Felt Reusable Surface Insulation (FRSI) and Low Temperature Reusable Surface Insulation (LRSI) on the Space Shuttle orbiter. It is easier to maintain and install, and it possesses a maximum operational temperature of 1200 ^{o}F[16]. The AFRSI concept modeled in this paper is composed of an outer fabric with C-9 coating, 6 lb/ft^3 Q-fiber felt insulation, and an inner fabric layer, and it is attached to the structure with RTV adhesive (Fig. 7). The weight and analysis models are based upon a 30 inch by 30 inch sample, and a summary of the weight model is contained in Appendix D, table 45. The material properties used for this model are found in Appendix C, tables 5, 7, 12, 13, 14, 15, and 27.

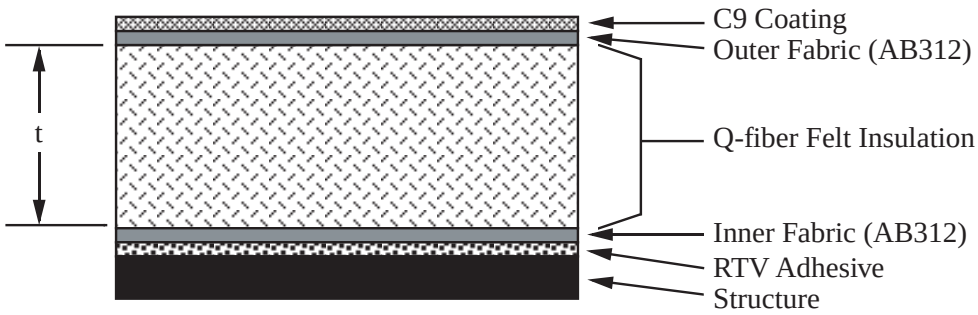

Figure 7. Depiction of the AFRSI thermal protection system.

Tailorable Advanced Blanket Insulation

Tailorable Advanced Blanket Insulation was developed by the NASA Ames Research Center as an improvement to the AFRSI currently certified on the Space Shuttle orbiter. Integrally woven corrugations provide higher strength and a higher operational temperature (2200 ^{o}F)[17] than AFRSI, and TABI is being proposed for use on the windward side of reentry vehicles[17]. The TABI considered here is composed of an outer ceramic fabric with C-9 coating, 6 lb/ft^3 Q-fiber felt insulation, ceramic fabric corrugations, and a fabric inner layer. It is attached to the structure with RTV adhesive (Fig. 8). The weight and analysis models examine a 30 inch by 30 inch sample, and a summary of the weight model is in Appendix D, table 46. The material properties for this model are found in Appendix C, tables 5, 7, 8, 9, 10, 11, 14, and 27.

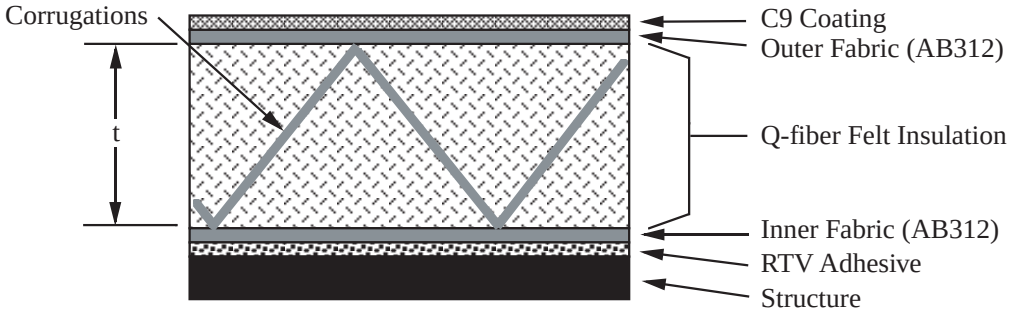

Figure 8. Depiction of the TABI thermal protection system.

Rigid Ceramic Tiles

Rigidized ceramic insulation tiles are used over the major portion of the Space Shuttle orbiter where temperatures range from 1300 to 2700 ºF[18]. Tiles have the highest temperature capabilities of the various TPS concepts considered in this study. The basic orbiter tile system is composed of a ceramic tile, a nomex (nylon) felt strain isolation mounting pad, and RTV adhesive. The LI-900 (9 lb/ft^3) and LI-2200 (22 lb/ft^3) tiles are coated on five sides to improve the surface emissivity and toughness and reduce catalycity. Due to the brittle nature and low strength of tiles, ceramic tile TPS must be isolated from the thermal and mechanical strains of the underlying structure. This is accomplished by the felt strain isolation pad (SIP). Strain isolation and thermal shock requirements limit the orbiter tiles to approximately 6 inch by 6 inch square footprints. The tiles have been susceptible to impact damage, and have required waterproofing after each flight[19]. Inspections, repairs, and waterproofing are time consuming and costly. Improved tile systems are under development which offer increased temperature capabilities and improved strength and durability. An example of this is the AETB tile with TUFI coating[9].

LI-900 (RSI) Tiles

LI-900 tiles are an all-silica, rigid, fibrous insulation system with a maximum operational temperature of 2300 ºF[18], and they are used extensively on the Space Shuttle orbiter. The rigid tile has a protective, emittance enhancing, and catalycity reducing RCG coating applied to the exposed surfaces, a densified region at the attachment to improve strength, and a SIP. It is attached to the structure with RTV adhesive (Fig. 9). For the weight and thermal models, the tiles are assumed to be 6 inches by 6 inches, and a summary of the weight model is contained in Appendix D, table 47. The material properties used for this model are found in Appendix C, tables 5, 16, 17, 18, 19, 20, and 27.

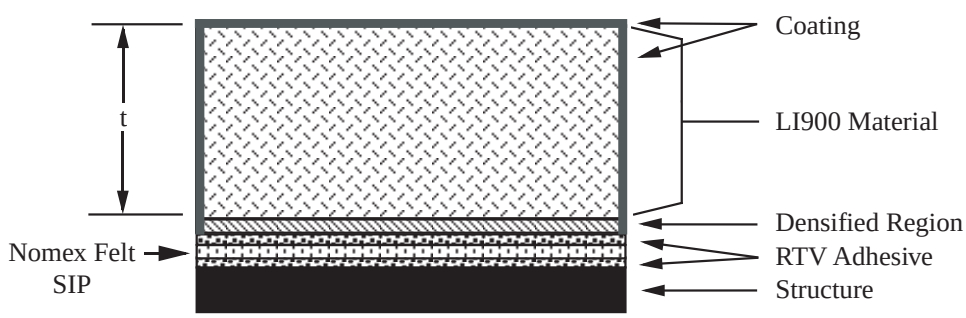

Figure 9. Depiction of the LI-900 thermal protection system.

Alumina Enhanced Thermal Barrier Tiles with TUFI Coating

The AETB ceramic tile with TUFI coating was developed at the NASA Ames Research Center as an improvement to the LI-900 tile. The AETB tiles demonstrate higher strength, added durability, and have a maximum operational temperature of 2500 ºF[9]. The system is composed of an 8 inch by 8 inch AETB ceramic tile that is coated with TUFI and mounted on a SIP (Fig. 10). Two tile densities, 8 lb/ft^3 (AETB-8) and 12 lb/ft^3 (AETB-12), are included in this study. Summaries of the weight models for AETB-8 and AETB-12 tiles are contained in tables 48 and 49 of Appendix D. The material properties used for these models are listed in Appendix C, tables 5, 18, 21, 22, 23, 24, 25, 26, and 27.

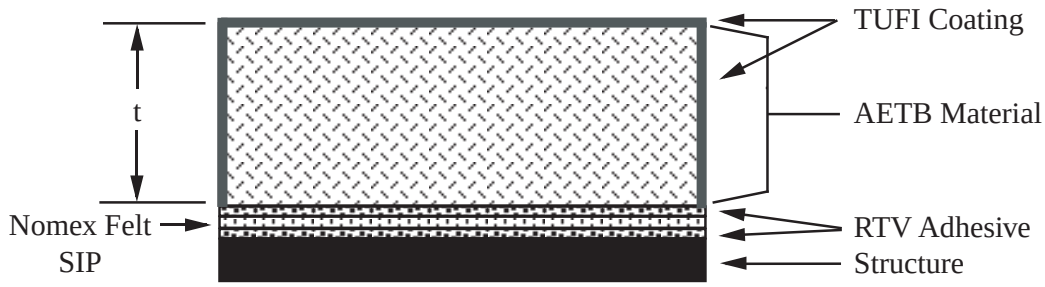

Figure 10. Depiction of the AETB thermal protection system.

Metallic Panels

Development of metallic thermal protection systems has been led by the NASA LaRC. The metallic TPS concepts considered in this study consist of a foil-gage metallic box encapsulating lightweight, fibrous ceramic insulation. The box rests upon an RTV and nomex felt edge support system to prevent flow from beneath the panels and is attached to the structure with mechanical fasteners. High temperature superalloys are used in the hottest regions, and titanium alloys are used in lower temperature applications to reduce weight. The outer face of the box, except for the multiwall concept, is constructed of a honeycomb sandwich to increase load carrying capability and durability. The weight of the metallic box is offset to some extent by the low density, efficient fibrous insulations used. The inherent ductility of the metallic materials used offers the potential for a more robust TPS, and the design can be easily modified to improve durability by making the facesheets thicker. In addition, the encapsulated designs are inherently waterproof, and the mechanical fasteners allow for easy removal and reattachment[11]. Metallic TPS panels do not, however, have the extensive flight history of the tiles and blankets, and the initial costs are expected to be high due to the required tooling. In addition, the spacecraft structure may require special design features to accommodate the mechanical fasteners.

Titanium Multiwall Thermal Protection System

TIMW is metallic insulation composed of alternate layers of flat and dimpled foil, enclosed by 0.003 inch titanium sidewalls[12]. The system is mechanically attached to the structure and rests upon a nomex felt edge support (Fig. 11). The maximum operational temperature is 1200 ^{o}F, and the weight and analysis models are based upon 12 inch by 12 inch panels. A summary of the weight model for titanium multiwall TPS is contained in Appendix D, table 50. The material properties used for this model are listed in Appendix C, tables 5, 18, 27, 28, 29, and 31.

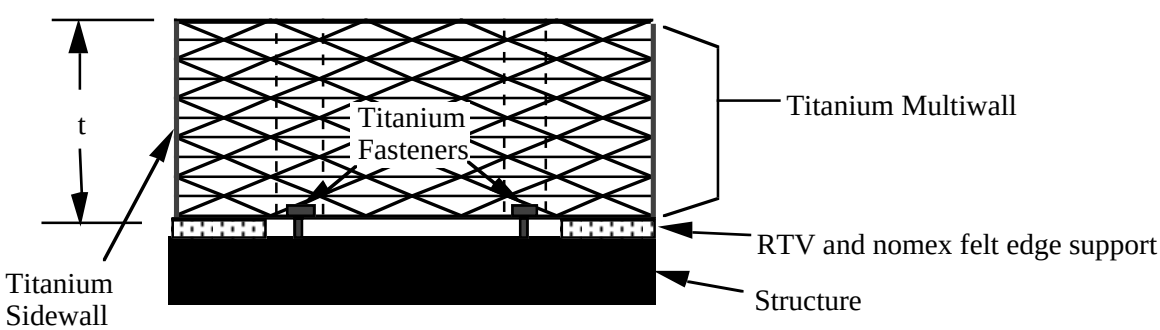

Figure 11. Depiction of the TIMW thermal protection system.

Superalloy Honeycomb Metallic Thermal Protection System

The SA/HC metallic TPS panels have been fabricated and have undergone extensive testing. The SA/HC metallic TPS incorporates lightweight insulation (Q-fiber and Cerrachrome) between two metallic honeycomb sandwich panels[13]. The outer sandwich is made of Inconel 617 (IN617), and the inner sandwich panel is made of titanium, and the system has a maximum operational temperature of 2000 °F. The sandwich panels are connected by 0.003 inch thick beaded IN617 sidewalls (Fig. 12). A summary of the weight model for a 12 inch by 12 inch SA/HC TPS is contained in Appendix D, table 51. The material properties for this model are listed in Appendix C, tables 5, 18, 27, 28, 29, 30, 32, 33, 34, 39, 40, 41, and 42.

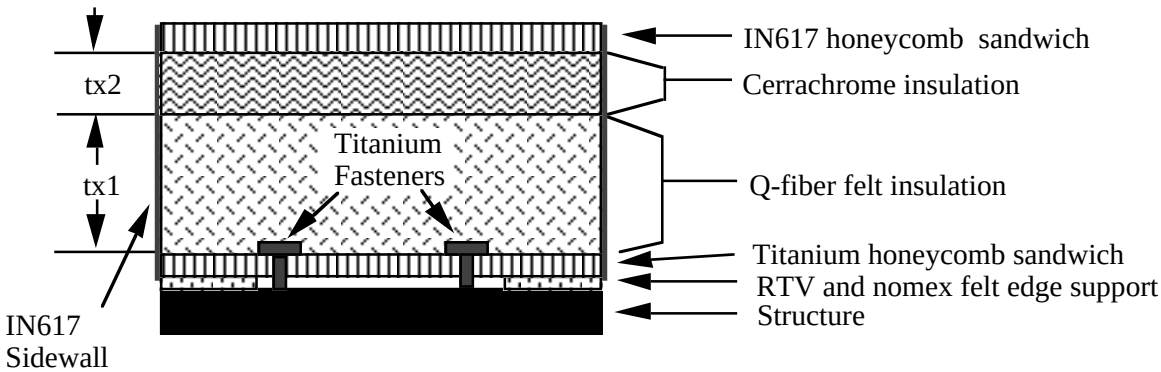

Figure 12. Depiction of the SA/HC metallic thermal protection system.

Second Generation Superalloy Honeycomb Metallic Thermal Protection System

The second generation superalloy honeycomb (SA/HC2) metallic TPS has been developed as an improvement to the superalloy honeycomb system. The layout of the SA/HC2 system is similar to the SA/HC, but it incorporates a lighter weight, higher temperature insulation (Saffil), and the structural weight has been reduced by replacing a 9 inch by 9 inch center section of the lower titanium sandwich with a thin foil[11] (Fig. 13). Both of these modifications reduce weight compared to the SA/HC concept. These panels which have been fabricated and tested have a predicted maximum operational temperature of 2000 °F. A summary of the weight model for 12 inch by 12 inch SA/HC2 TPS panels is contained in Appendix D, table 52. The material properties for this model are listed in Appendix C, tables 5, 18, 27, 28, 29, 30, 32, 33, 34, 37, and 38.

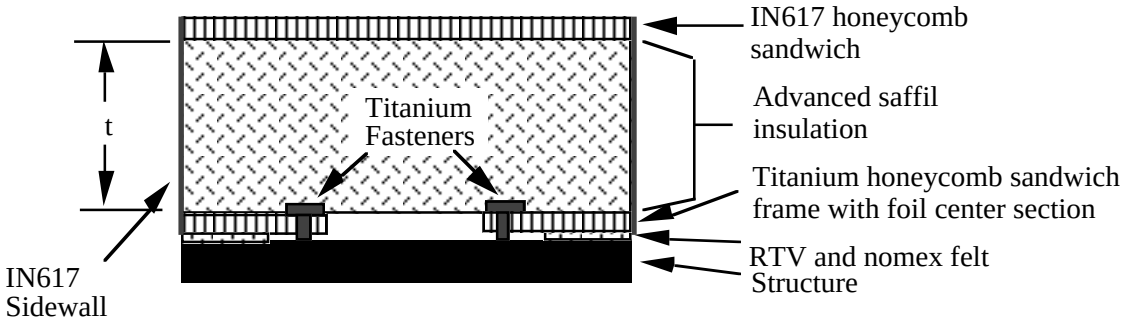

Figure 13. Depiction of SA/HC2 metallic TPS system.

Titanium Honeycomb Metallic TPS

The titanium honeycomb (TI/HC) metallic TPS concept is a reduced weight metallic TPS concept for lower temperature applications. The TI/HC TPS panel replaces the IN617 components of the SA/HC2 concepts with titanium members (Fig. 14). The material change, which has not been rigorously analyzed or tested, results in a weight savings of 0.37 lb/ft^2 as compared to the Advanced Superalloy Honeycomb TPS. The system has a maximum operational temperature of 1200 ^{o}F . A summary of the weight model for 12 inch by 12 inch TI/HC TPS panel is contained in Appendix D, table 53. The material properties used for this concept are listed in Appendix C, tables 5, 18, 27, 28, 29, 30, 39, and 40.

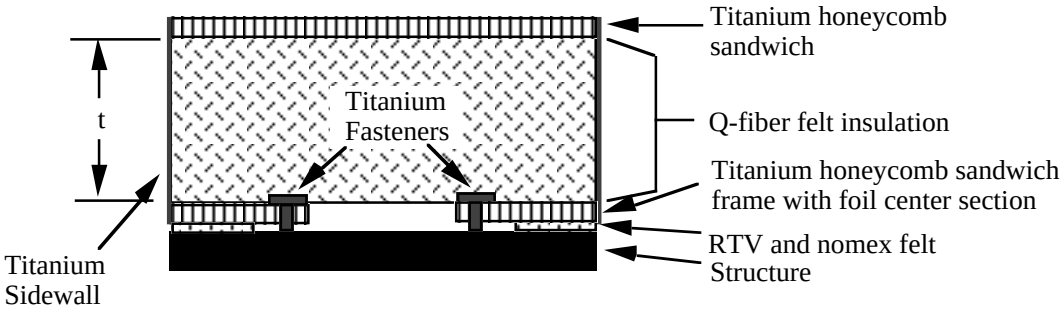

Figure 14. Depiction of the TI/HC metallic TPS system.

Advanced Metallic Honeycomb Thermal Protection System

The Advanced Metallic Honeycomb thermal protection system (AMHC) is being proposed at the NASA LaRC as an improvement to the superalloy honeycomb metallic system. It incorporates an advanced, low conductivity Internal Multiscreen Insulation (IMI) between an outer PM2000 honeycomb sandwich and a thin titanium facesheet on the bottom[11]. A box frame that runs along the outer edges is attached to the lower facesheet. The frame and bottom facesheet configuration replace the honeycomb sandwich to reduce structural weight, and a PM2000 honeycomb replaces the Inconel 617 honeycomb panel because it has the potential to increase the maximum operational temperature to 2200 ^{o}F and has a lower density. The 12 inch by 12 inch system is fastened to bosses on the structure with a quick release spring (Fig. 15). This new fastening configuration will allow the TPS to be examined and repaired much more quickly. A summary of the weight model for AMHC TPS is contained in Appendix D, table 54. The material properties for the AMHC system are listed in Appendix C, tables 5, 18, 27, 28, 29, 34, 35, 36, 43, and 44. It is important to note that no detailed design has been performed on this concept, and the multilayer insulation properties are predicted from analytical models.

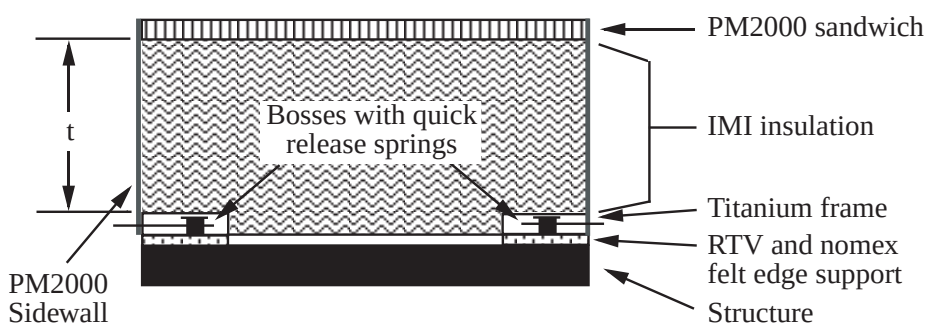

Figure 15. Depiction of the Advanced Metallic Honeycomb (AMHC) thermal protection system.

PARAMETERS INVESTIGATED

Heat Load

The TPS concepts are sized using variations of the baseline heat flux profiles for the Access to Space (ATS) reference vehicle[20] and the proposed Reusable Launch Vehicle (RLV) phase 1 preliminary environments[1]. Two different vehicles are investigated to broaden the applicability of the results. The trajectory profiles were flown with a low heating rate and high heating load which may penalize the ceramic concepts which can handle higher temperatures. The baseline heat flux profiles for two specific locations on each of these two vehicles are shown in figures 16 and 17. Heat flux profiles for surface locations with peak radiation equilibrium temperatures of approximately 1100 ^{o}F and 1850 ^{o}F are chosen on each vehicle to provide heating rates suitable for a range of TPS concepts. The reference body points investigated for ATS are at x=29.3 ft along the side of the vehicle (body point B on Fig. 16) and at x=20.8 ft along the windward surface (body point A on Fig. 16), both with exposure times of 2500 s. For the RLV, the body points at x=11.6 ft and x=112.1 ft, on the windward surface, (body points A and B, respectively on Fig. 17) with exposure times of 2500 s are investigated. The heat load represented by body point B on figure 17 is the same heat load which was represented in figure 5.

The influence the total heat load has on TPS weight is investigated by varying either the magnitude of the heat flux or the integrated time from 0.25 to 2.0 times the reference heat profiles. When the integrated time is varied, the radiation equilibrium temperature remains constant (table 1). In this study, all TPS concepts are within their temperature limits. When the magnitude of the heat flux is expanded, the maximum radiation equilibrium temperature varies within the parametric range (table 2). In some instances, the temperature exceeds the TPS temperature limit, and TPS weights are not calculated in these cases. All other parameters are held at the baseline values.

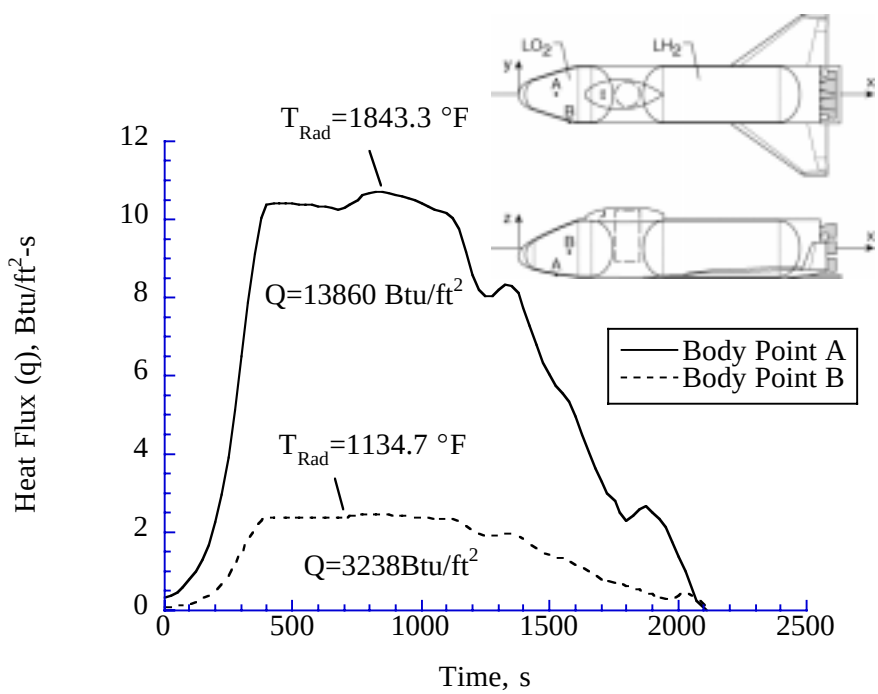

Figure 16. Baseline Heat flux profiles for ATS body points.

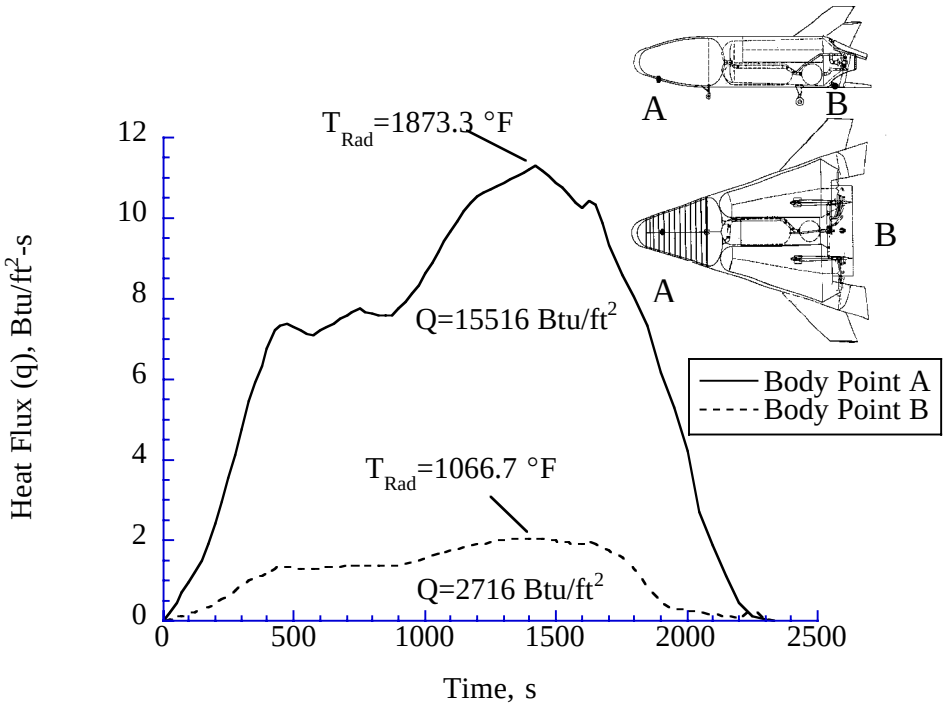

Figure 17. Baseline Heat flux profiles for RLV body points.

Table 1. Heat Load Range (Integrated Time Scaled)

	0.25 x Baseline Profile		Baseline Profile		2 x Baseline Profile	
Heating Profile	Heat Load(Q) Btu/ft^2	T_{Rad} °F	Heat Load (Q) Btu/ft^2	T_{Rad} °F	Heat Load (Q) Btu/ft^2	T_{Rad} °F
ATS-A	3460	1843	13860	1843	27720	1843
ATS-B	810	1135	3238	1135	6476	1135
RLV-A	3879	1873	15516	1873	31032	1873
RLV-B	679	1067	2716	1067	5432	1067

Table 2. Heat Load Range (Heat Flux Magnitude Scaled)

	0.25 x Baseline Profile		Baseline Profile		2 x Baseline Profile	
Heating Profile	Heat Load(Q) Btu/ft^2	T_{Rad} °F	Heat Load (Q) Btu/ft^2	T_{Rad} °F	Heat Load (Q) Btu/ft^2	T_{Rad} °F
ATS-A	3460	1169	13860	1843	27720	2279
ATS-B	810	668	3238	1135	6476	1434
RLV-A	3879	1190	15516	1873	31032	2315
RLV-B	679	620	2716	1067	5432	1356

Structural Heat Capacity

To investigate the effect the structural heat capacity, C_p , has on TPS weight, the structural thickness of the underlying tank wall is varied from 0.025 inch to 0.2 inch from the reference value of 0.10 inch. The total structural heat capacity is directly proportional to the thickness, t, because the density, ρ, and specific heat capacity, c_p, are constant for aluminum at 300 °F (equation 1).

$$C_p = c_p \rho t \qquad (1)$$

This corresponding structural heat capacity range is shown in table 3. The heat flux profile was held at the baseline for each body point examined.

Table 3. Structural Heat Capacity Range

0.25 x Baseline Capacity	Baseline Capacity	2 x Baseline Capacity
Heat Capacity (C_p) Btu/ft^2-°R	Heat Capacity (C_p) Btu/ft^2-°R	Heat Capacity (C_p) Btu/ft^2-°R
0.082	0.327	0.654

RESULTS

Results demonstrate the relationship between TPS thickness and weight for each concept, and parametric weight comparisons among TPS concepts. The weight comparisons demonstrate the effect of integrated heat load, maximum heat flux, and structural heat capacity. Trajectories from two vehicles are examined to see if the results are affected. The benefits of applying additional improvements to the AMHC TPS concept are also assessed.

Dependence of TPS Weight on TPS Thickness

The component weights for each TPS concept are listed in appendix D. Figures 18 and 19 summarize TPS weight as a function of TPS thickness for each concept. Figure 18 is a plot of the TPS concepts for use at relatively low temperatures (less than 1400 °F) while figure 19 shows TPS concepts for use at higher temperatures. For reference, two TPS concepts (TABI and LI-900) are plotted in both figures. It should be noted that these plots are independent of the heat flux profile used. For a given TPS thickness, the weight is calculated using a formula within the 1-D sizing code. These data are presented for two reasons. First, these plots may be used to determine the corresponding TPS thicknesses for the TPS weight data points presented in the subsequent figures. Secondly, these plots can provide insight into the relative performances of the various TPS concepts. An important trend in figures 18 and 19 is that the metallic TPS with durable outer panels and efficient interior insulation (TI/HC, SA/HC, SA/HC2, and AMHC) are more weight competitive as their thickness increases. The reason for this is that these systems are designed with the outer honeycomb sandwich panel thickness being constant. At low total heat load conditions, small amounts of insulation are required. Because the panel weight is predominantly comprised of thermally inefficient honeycomb panels, metallic TPS have higher effective densities than blankets and tiles. However as more insulation is required, the light interior insulation thickness is increased, and the effective density of the metallic concepts is decreased, and they become more efficient. These trends may be seen in both figures 18 and 19 as well as the subsequent parametric weight comparison plots.

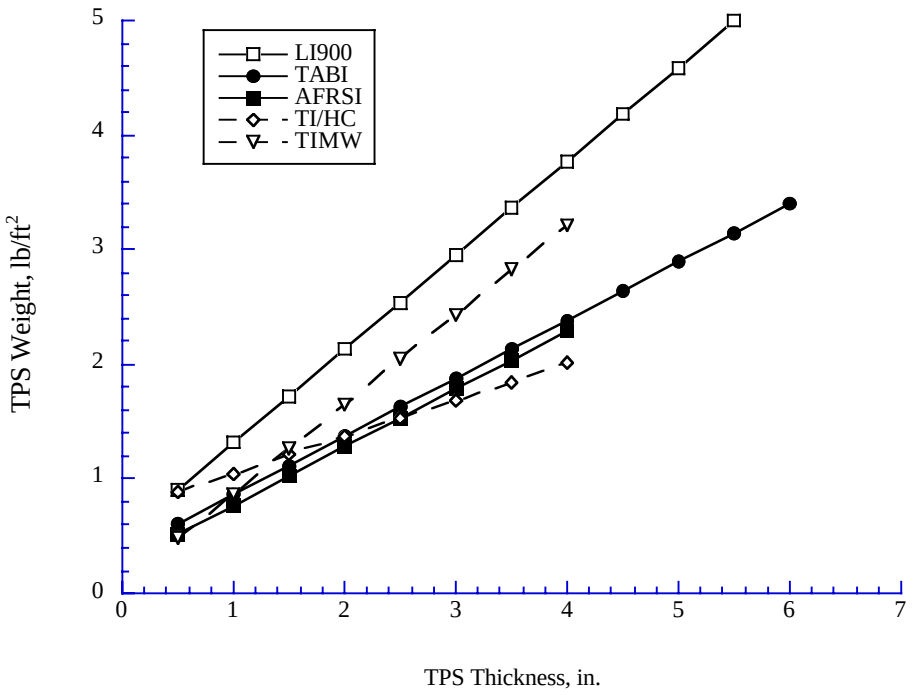

Figure 18. Lower temperature TPS weight versus TPS thickness.

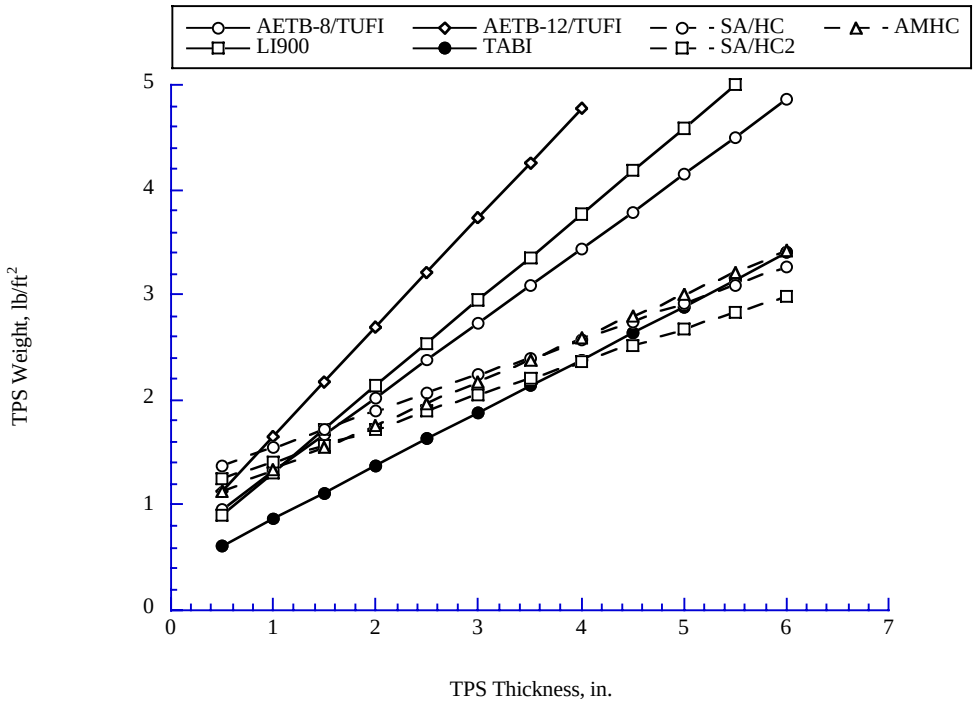

Figure 19. Higher temperature TPS weight versus TPS thickness.

Dependence of TPS Weight on Trajectory and Configuration

Heat flux profiles for the Access to Space (ATS) and a proposed Reusable Launch Vehicle (RLV) are studied to investigate the effect of trajectory on required TPS weight. TPS weights for a ceramic blanket, ceramic tile, and metallic panel are plotted versus heat load when the magnitude of the heat flux profiles is varied from 0.5 to 2 times the baseline heat flux profiles (Figs. 16 and 17). If the TPS weight curves are identical for both vehicles, then only one vehicle trajectory will be required for the parametric studies. The results shown in figure 20 indicate that the weight curves are similar but slightly offset for the two different trajectories. For completeness, TPS weight comparisons are generated for both vehicle trajectories.

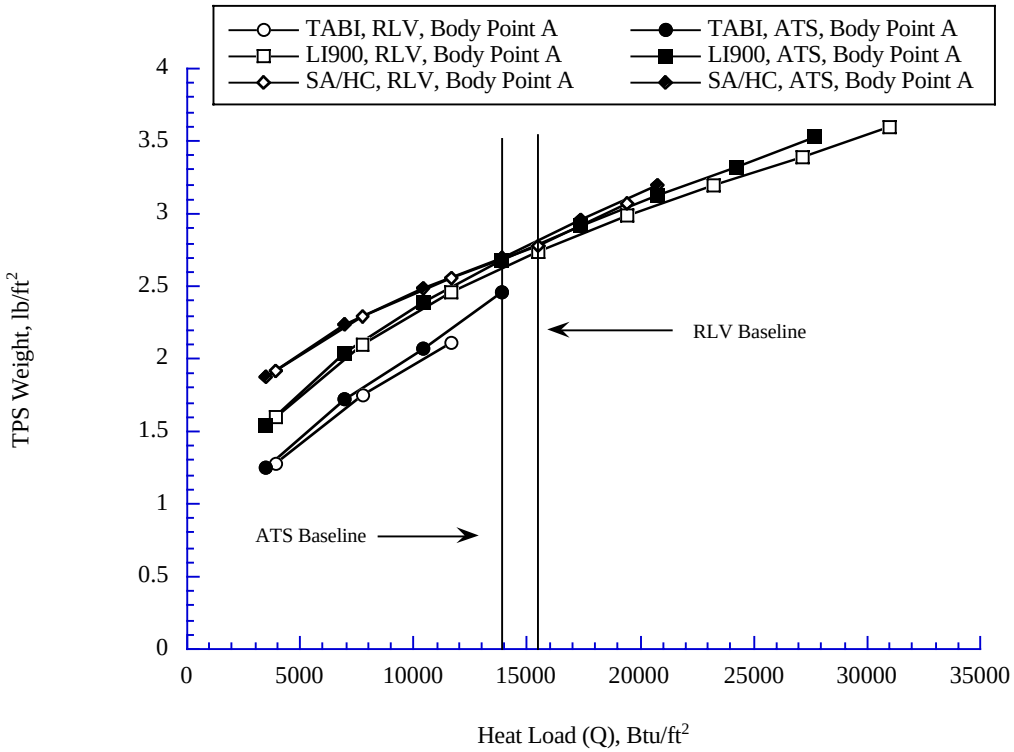

Figure 20. TPS concept weight versus heat load for two higher temperature heating profiles.

Dependence of TPS Weight on Heat Load (Time Integration Scaled)

The influence the total heat load has on TPS weight is first investigated by scaling the integrated exposure time of the TPS to the baseline heating profile from 0.5 to 2 times the reference exposure time. The corresponding parametric range, along with the radiation equilibrium temperatures, is shown in table 1. For the lower heating profiles, TPS weights for low temperature TPS concepts are shown on figure 21 and figure 22. From these plots, it is apparent that the ceramic blanket concepts (AFRSI and TABI) are the lightest concepts, and TIMW is only competitive for very low heat loads. LI-900 and TI/HC have nearly the same weight at the baseline heating. As the heat load decreases, LI-900 becomes the lighter of the two concepts, and as the heat load increases, TI/HC becomes lighter than LI-900.

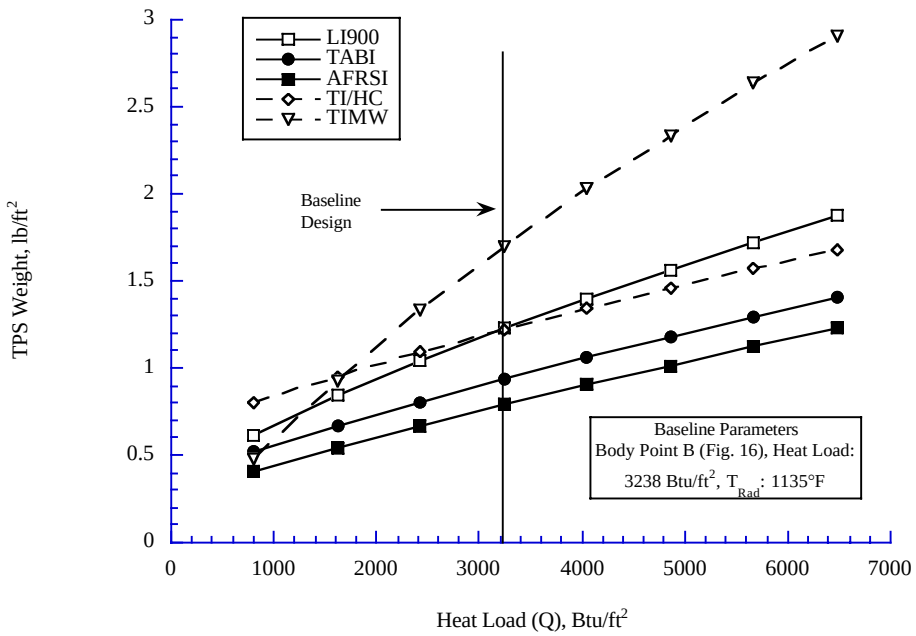

Figure 21. Lower temperature TPS weight versus heat load with scaled time for ATS.

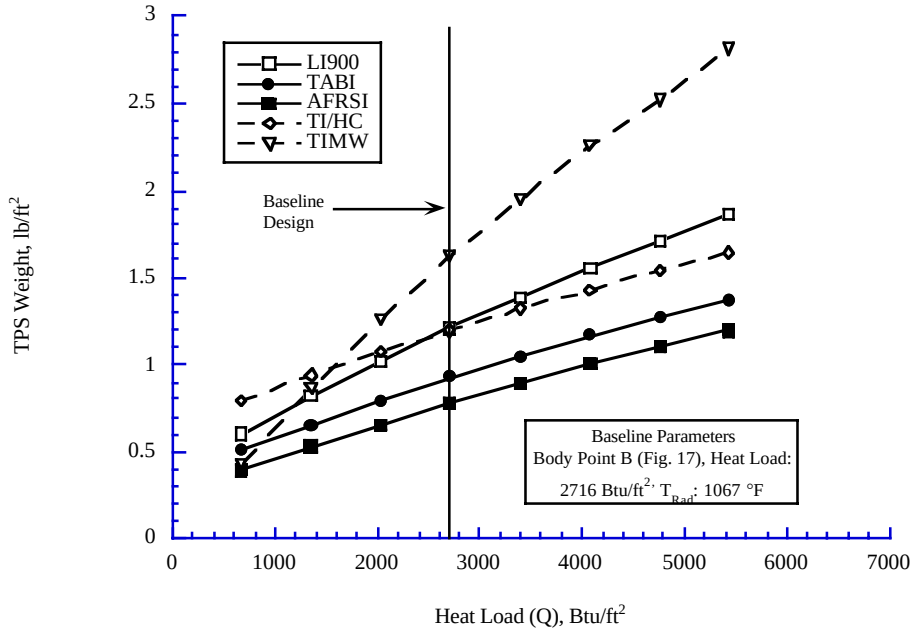

Figure 22. Lower temperature TPS weight versus heat load with scaled time for RLV.

For the higher heating profiles, TPS weight versus heat load is plotted on figures 23 and 24. From these plots, AMHC is the lightest TPS concept over about 90% of the parametric range. In addition, SA/HC and SA/HC2 are lighter than all the tiles as the heat load increases above the reference heat profiles, while LI-900 is lighter than the SA/HC and the SA/HC2 as the heat load decreases below the

reference heat profiles. If SA/HC and SA/HC2 are compared to AETB-8/TUFI and AETB-12/TUFI, the figures indicate that the metallic panels are lighter over the majority of the range. Finally, TABI is heavier than AMHC over a majority of the range, and lighter than the tiles.

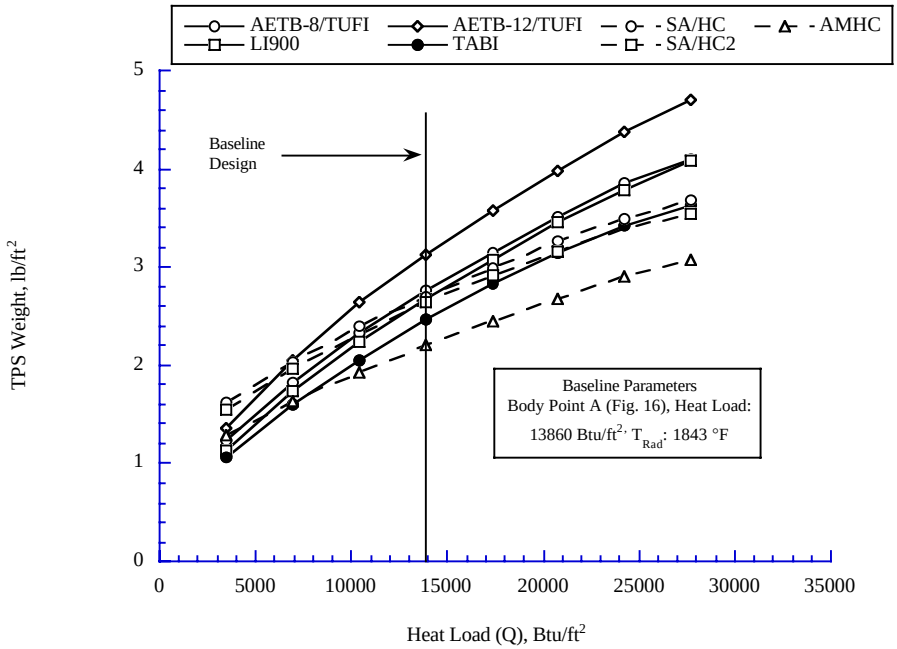

Figure 23. Higher temperature TPS weight versus heat load with scaled time for ATS.

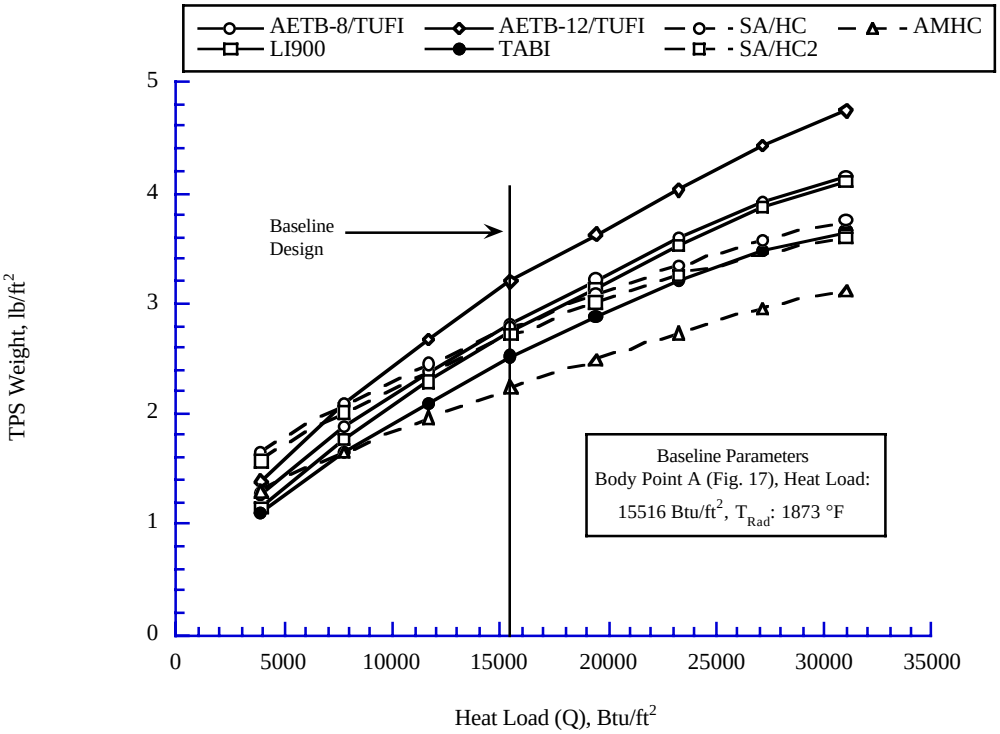

Figure 24. Higher temperature TPS weight versus heat load with scaled time for RLV.

Dependence of TPS Weight on Heat Load (Maximum Heat Flux Scaled)

The influence the total heat load has on the TPS weight is also investigated by scaling the magnitude of the heat flux profile from 0.5 to 2 times the reference heat flux profile (Figs. 16 and 17). The corresponding parametric range, along with the radiation equilibrium temperature within the parametric range, is shown in table 2. Because the trends are the same for both vehicles examined, the results for only ATS is shown. For the lower heating profiles, TPS weights for low temperature TPS concepts are shown on figure 25. From this plot, it is apparent that the ceramic blanket concepts (AFRSI and TABI) are the lightest concepts, and TIMW is competitive over only a relatively small area. LI-900 and TI/HC have nearly the same weight at the baseline. As the heat load decreases, LI-900 becomes the lighter of the two concepts. However as the heat load increases, TI/HC becomes lighter, but can only be used up to the point where its maximum allowable temperature is not exceeded.

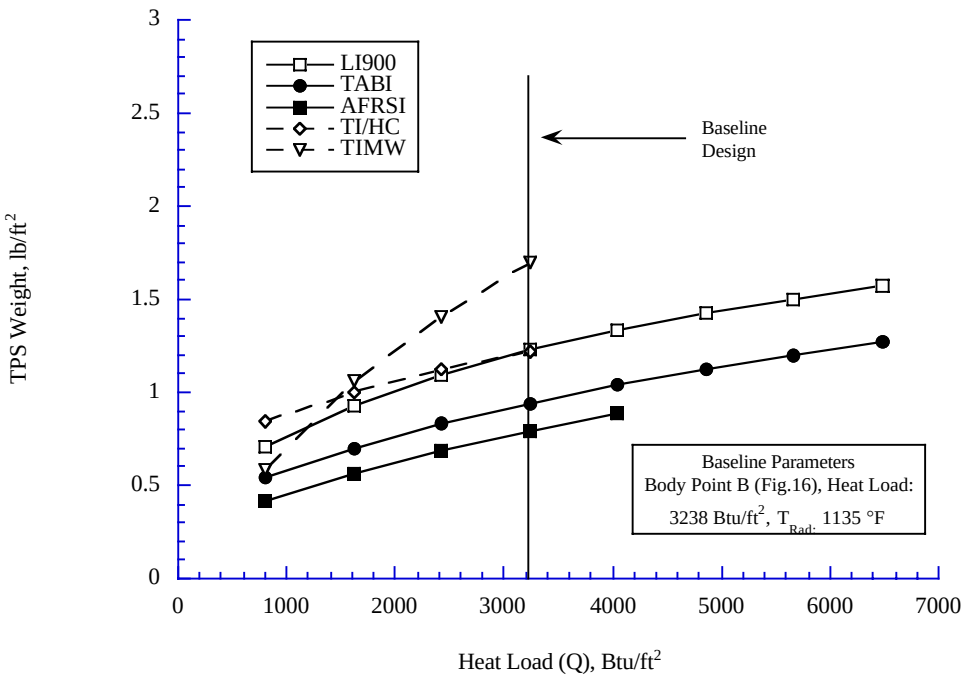

Figure 25. Lower temperature TPS weight versus heat load with scaled heat flux for ATS.

For the higher heating profiles, TPS weight versus heat load is plotted on figure 26. From this plot, TABI and AMHC are the lightest TPS concepts over their useful temperature range. LI-900, AETB-8, SA/HC2, and SA/HC have comparable weights over most of the parametric range, but the tiles are the only concepts capable of operation over the entire heating range. Finally, AETB-12 is the heaviest concept over the entire range.

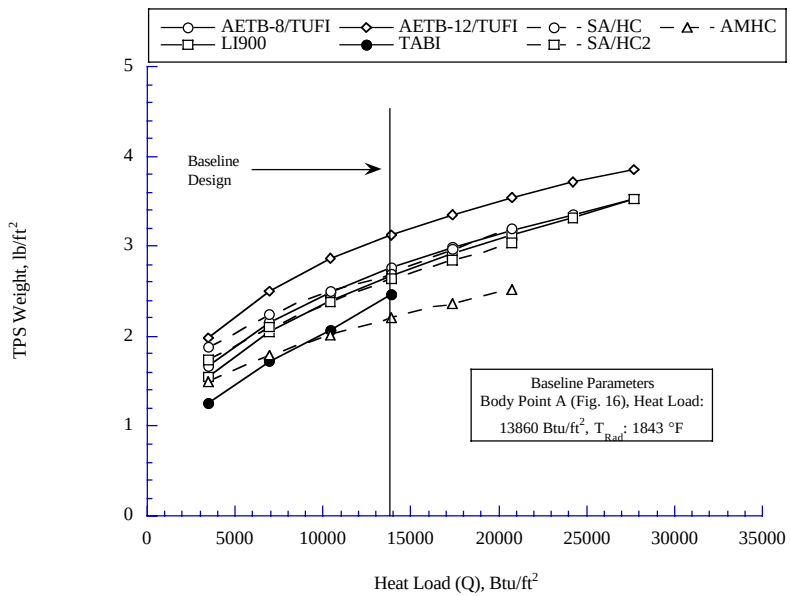

Figure 26. Higher temperature TPS weight versus heat load with scaled heat flux for ATS.

Dependence of TPS Weight on Structural Heat Capacity

To investigate the effect that total structural heat capacity, C_p , has on TPS weight, the structural thickness was varied from 0.025 inch to 0.2 inch from the reference value of 0.10 inch. The corresponding structural heat capacity range is shown in table 3. The heat flux profile is held at the baseline for each body point examined. For the lower heating profiles, TPS weights for low temperature TPS concepts are shown on figure 27. From this plot, it is apparent that the ceramic blanket concepts (AFRSI and TABI) are the lightest concepts, and TIMW is heavier over the entire range. LI-900 and TI/HC have nearly the same weight at the baseline. As C_p increases, LI-900 becomes the lighter of the two concepts. However as C_p decreases, TI/HC becomes lighter.

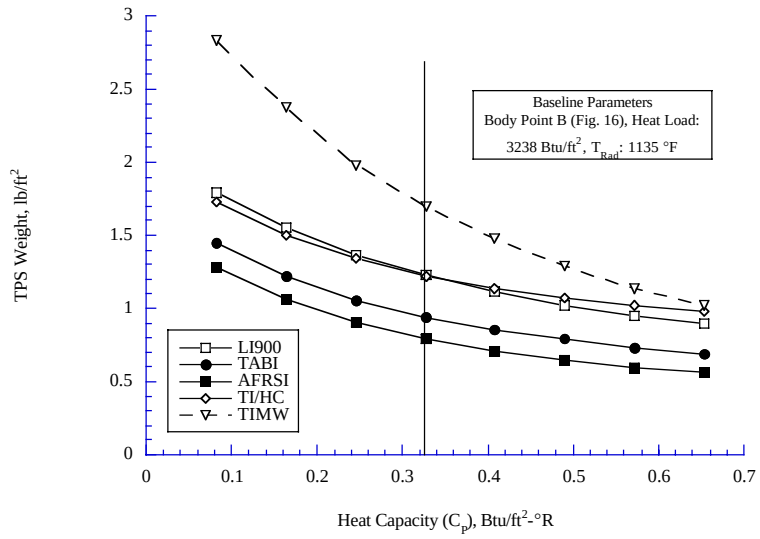

Figure 27. Lower temperature TPS weight versus structural heat capacity for ATS.

For the higher heating profiles, high temperature TPS weights versus structural heat capacity are plotted on figure 28. From this plot, AMHC is the lightest TPS concept over the parametric range while TABI is the second lightest. Once again, LI-900, AETB-8, SA/HC2, and SA/HC have comparable weights over the parametric range, and AETB-12 is considerably heavier.

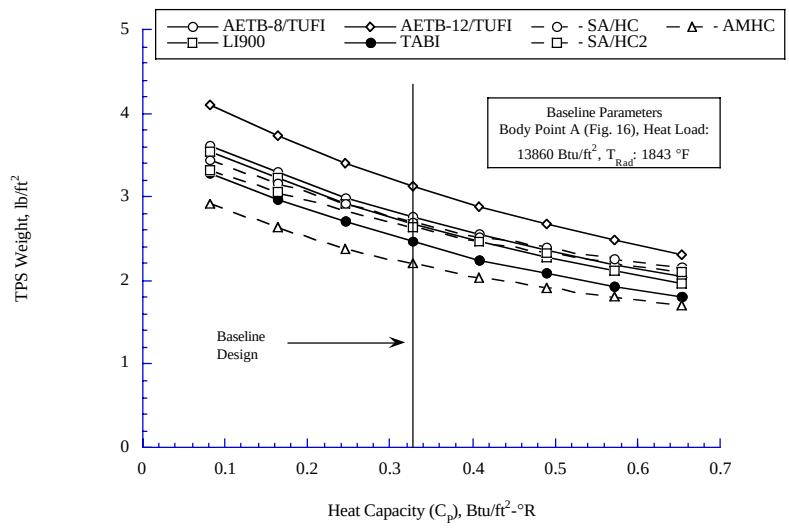

Figure 28. Higher temperature TPS weight versus structural heat capacity for ATS.

AMHC TPS Weight Improvement Estimate

Two additional improvements to the AMHC TPS offer the potential for further weight savings: a higher emissivity coating and larger panels. To obtain an upper bound to the projected weight savings, the weight of the coating was neglected, and the panel was not resized for increased structural loads (this is beyond the scope of the current study). The weights for the AMHC baseline panel, the panel with the high emittance coating (0.85), the larger (18 inch-square) panel, and the larger panel with the high emittance coating are shown in figure 29. The combined improvements may reduce the weight by as much as 13 percent.

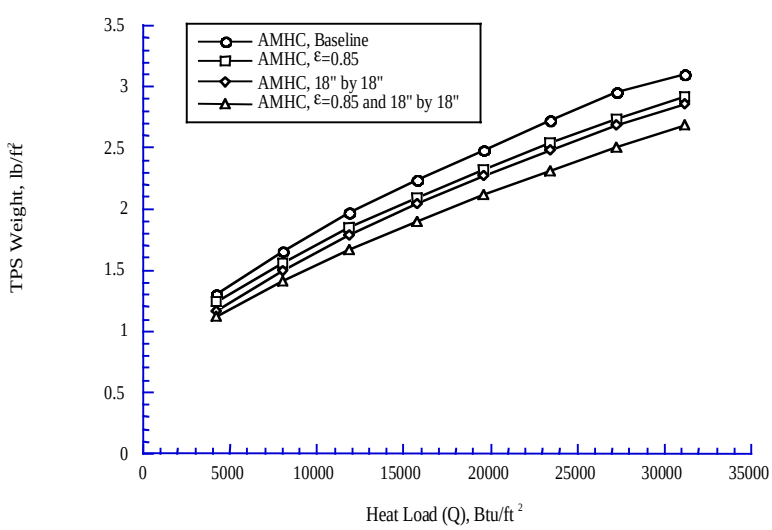

Figure 29. Potential AMHC weight savings due to design improvements.

CONCLUSIONS

A parametric assessment of the weight of advanced metallic, ceramic blanket and ceramic tile thermal protection systems (TPS) was conducted using an implicit, one-dimensional (1-D) finite element sizing code. TPS concepts were sized for heating profiles from two vehicles, the Access to Space (ATS) vehicle and a proposed Reusable Launch Vehicle (RLV), to investigate whether TPS weight comparison trends varied with trajectory. The applied heat load and structural heat capacity were varied to compare the weight of TPS concepts over a wide range of conditions. Temperature distributions calculated using the 1-D TPS sizing code were compared with results from detailed two-dimensional (2-D) models to show that the 1-D thermal model results were accurate for sizing each TPS concept.

Although the TPS weight for a given heat load varied slightly for the different trajectories considered, the same weight comparison trends were observed for both vehicles. Therefore the trends identified in this study may not be unique to the trajectories considered.

Among the TPS concepts considered for the lower temperature regime, several trends were observed. The blanket TPS concepts are lighter than competing concepts for almost all conditions considered. AFRSI is the lightest, and TABI is only slightly heavier. At very low integrated heat loads, Titanium Multiwall (TIMW) is weight competitive with blanket concepts, but because of its relatively high thermal conductivity it is not competitive for most of the conditions considered. At the baseline conditions, Titanium Honeycomb panels (TI/HC) and LI-900 tiles are approximately the same weight. As the heat load increased or the structural heat capacity decreased, the TI/HC became the lighter of the two. However, as the heat load decreased or the structural heat capacity increased, the LI-900 became the lighter of the two.

For the higher heating profiles, the AMHC metallic concept is generally the lightest concept, while TABI is generally the second lightest. In addition, the LI-900 tiles, the AETB-8 tiles, the Superalloy Honeycomb (SA/HC) and Advanced Superalloy Honeycomb (SA/HC2) metallic concepts had comparable weights over the parametric ranges. In general, the metallic concepts perform better with increasing integrated heat load due to the low density fibrous insulations used in these concepts, but the tiles have a higher temperature capability. The AETB-12 tiles proved to be heavier over nearly all the parameter ranges.

This study has compared TPS weights for several concepts over a wide range of conditions. Although low weight is a very important parameter, it is only one of several competing requirements for future TPS, including durability, operability, rapid turnaround, low maintenance, and low life cycle cost. Metallic TPS, which are shown to be weight competitive with other TPS concepts in this study also have the potential to better meet the additional requirements of future TPS. The AMHC metallic concept appears to be very promising, but this concept requires additional design work and experimental verification of its performance.

REFERENCES

1. Baumgartner, Robert I.: VentureStar™ Single Stage to Orbit Reusable Launch Vehicle Program Overview. *Proceedings of the Space Technology and Applications International Forum*, Vol. 3, Albuquerque, NM, Jan. 1997, pp. 1033-1039.

2. Chase, R. L.: Comments on a Military Transatmospheric Aerospace Plane. *Proceedings of the Space Technology and Applications International Forum*, Vol. 3, Albuquerque, NM, Jan. 1997, pp. 1185-1194.

3. Penn, Jay P.; and Lindley, Charles A.: Space Tourism Optimized Reusable Spaceplane Design. *Proceedings of the Space Technology and Applications International Forum*, Vol. 3, Albuquerque, NM, Jan. 1997, pp. 1073-1090.

4. Cook, Layne M.; and Ball, Jim: High-Alpha Space Trucks. *Proceedings of the Space Technology and Applications International Forum*, Vol. 3, Albuquerque, NM, Jan. 1997, pp. 1119-1124.

5. Andrews, Dana; Paris, Steve; and Rubeck, Mark: Suborbital Freight Delivery Concept Exploration. *Proceedings of the Space Technology and Applications International Forum*, Vol. 3, Albuquerque, NM, Jan. 1997, pp. 1025-1031.

6. Hunt, James L.; Lockwood, Mary Kae; Petley, Dennis H.; and Pegg, Robert J.: Hypersonic Airbreathing Vehicle Visions and Enhancing Technologies. *Proceedings of the Space Technology and Applications International Forum*, Vol. 3, Albuquerque, NM, Jan. 1997, pp. 1285-1295.

7. Morris, W. D.; White, N. H.; and Ebeling, C. E.: Analysis of Shuttle Orbiter Reliability and Maintainability Data for Conceptual Studies. AIAA Paper 96-4245, *AIAA Space Programs and Technology Conference*, Huntsville, AL, Sept. 24-26, 1996.

8. Rasky, Daniel J.: Advanced Ceramic Matrix Composites for TPS. *Current Technology for Thermal Protection Systems*. NASA Conference Publication 3157, 1992, pp. 43-62.

9. Hinkle, Karrie A.; Staszak, Paul R.; and Watts, E. T.: Advanced Ceramic Materials Development and Testing. AIAA Paper 96-1527, *37th Structures, Structural Dynamics, and Materials Conference*, 1996, pp. 525-530.

10. Lu, I. Tina: TABI - The Lightweight Durable Thermal Protection System for Future Reusable Launch Vehicles. AIAA Paper 96-1426, *37th Structures, Structural Dynamics, and Materials Conference*, 1996, pp. 957-961.

11. Blosser, M. L.: Development of Metallic Thermal Protection Systems for the Reusable Launch Vehicle. *Proceedings of the Space Technology and Applications International Forum*, Vol. 3, Albuquerque, NM, Jan. 1997, pp. 1125-1143. Also published as NASA TM X-110296, Oct. 1996.

12. Jackson, L.R.; and Dixon, S. C.: *A Design Assessment of Multiwall, Metallic Stand-off, and RSI Reusable Thermal Protection Systems Including Space Shuttle Application*. NASA TM X-81780, 1980.

13. Blair, W.; Meaney, J. E.; and Rosenthal, H. A.: *Fabrication of Prepackaged Superalloy Honeycomb Thermal Protection System (TPS) Panels.* NASA CR-15646, Oct. 1985.

14. Whetstone, W. D.: *EISI-EAL Engineering Analysis Language Reference Manual, System Level 312*. Engineeringing Information Systems, Incorporated, San Jose, 1983.

15. *TPSX: Thermal Protection Systems Expert and Material Database*, Vers. 1.1, Rev. Feb. 1998. http:// asm.arc.nasa.gov/tpsx11.shtml Accessed Jan 18, 2000.

16. Cleland, John; and Iannetti, Francesco: *Thermal Protection System of the Space Shuttle*, NASA CR- 4227, 1989.

17. Chiu, S. Amanda; and Pitts, William C.: Reusable Surface Insulation for Reentry Spacecraft. AIAA Paper 91-0695, *29th Aerospace Sciences Meeting*, Jan. 1991.

18. Williams, S. D.; and Curry, Donald M.: *Thermal Protection Materials, Thermophysical Property Data*. NASA Reference Publication 1289, 1992.

19. Korb, L. J.; Marant, C. A.; Calland, R. M.; and Thatcher, C. S.: The Shuttle Orbiter Thermal Protection System. *American Ceramic Society Bulletin*, Vol. 60, No. 11, 1981, pp. 1188-1193.

20. *Access to Space Advanced Technology Team Final Report*. NASA Langley Research Center, Vol.3 Design Data, July 1993.

21. Bouslog, S. A.; Moore, B.; Lawson, I.; and Sawyer, J. W.: X-33 Metallic TPS Tests in NASA-LaRC High Temperature Tunnel. AIAA Paper 99-1045, *37th AIAA Aerospace Sciences Meeting and Exhibit*, Jan. 1999.

22. Gorton, M.P.; Shideler, J. L.; and Webb, G. L.: *Static and Aerothermal Tests of a Superalloy Honeycomb Prepackaged Thermal Protection System*. NASA TP-3257, 1993.

23. Blair, W.; Meaney, J. E.; and Rosenthal, H. A.: *Re-Design of Titanium Multi-Wall Thermal Protection System Test Panels*. NASA CR-172247, 1984.

24. *Aerospace Structural Metals Handbook*, CINDAS/USAF CRDA Handbooks Operation. Purdue University, West Lafayette, IN, 1994.

APPENDIX A

METALLIC THERMAL PROTECTION SYSTEM FOR THE X-33

Metallic panels comprise the majority of the thermal protection system for the X-33 vehicle. The X-33 metallic TPS[21] shares similar materials, thicknesses, and fabrication techniques with the metallic TPS described and analyzed in this paper. However, the X-33 TPS is significantly different in configuration.

Typical X-33 metallic TPS panels are shown in figure 30. The outer surface is composed of foil-gauge, honeycomb sandwich made from high temperature superalloy or oxide dispersion strengthened (ODS) alloy metal. Metallic foil seals are attached to the outer honeycomb sandwich to prevent hot gas ingress between panels. Foil-encapsulated insulation is attached to the inner surface of the honeycomb sandwich. High temperature attachment rosettes, located at the corners of the panels, connect the outer honeycomb sandwich to the underlying support structure. A significant gap exists between the foil-encapsulated insulation and the vehicle structure. The resulting configuration is considerably more complicated than the other TPS concepts analyzed in this study and is not directly comparable. A fair comparison would require design and analysis of the TPS, TPS support system, and cryogenic tank structure—a task beyond the scope of this study. Therefore, the X-33 metallic TPS was not included.

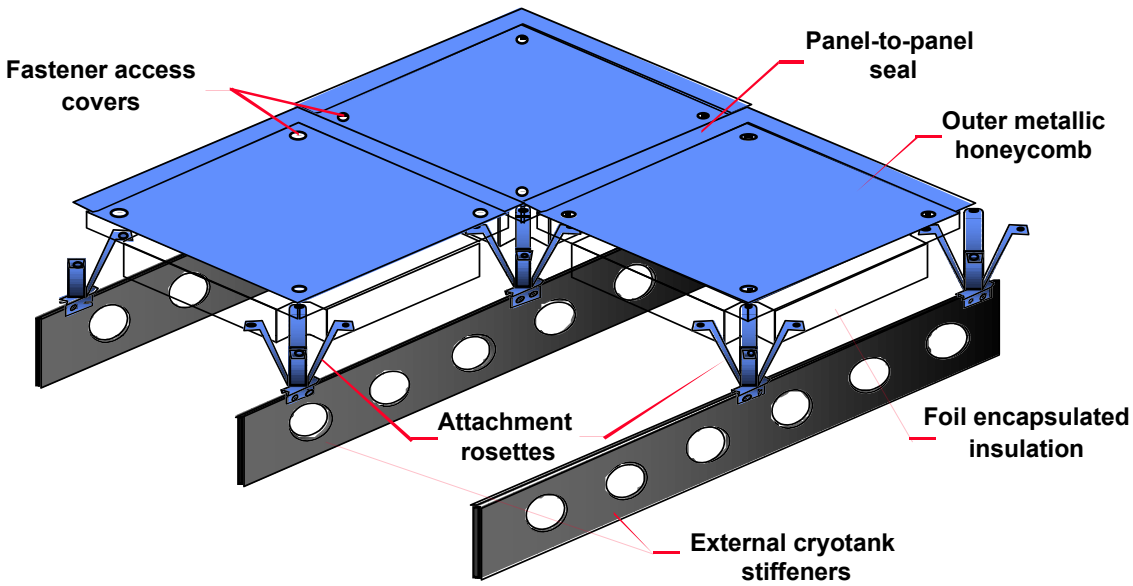

Figure 30. X-33 metallic TPS panel concept and attachment to the vehicle.

APPENDIX B

Comparison of 1-D Analysis Model Results with 2-D Detailed Model Results

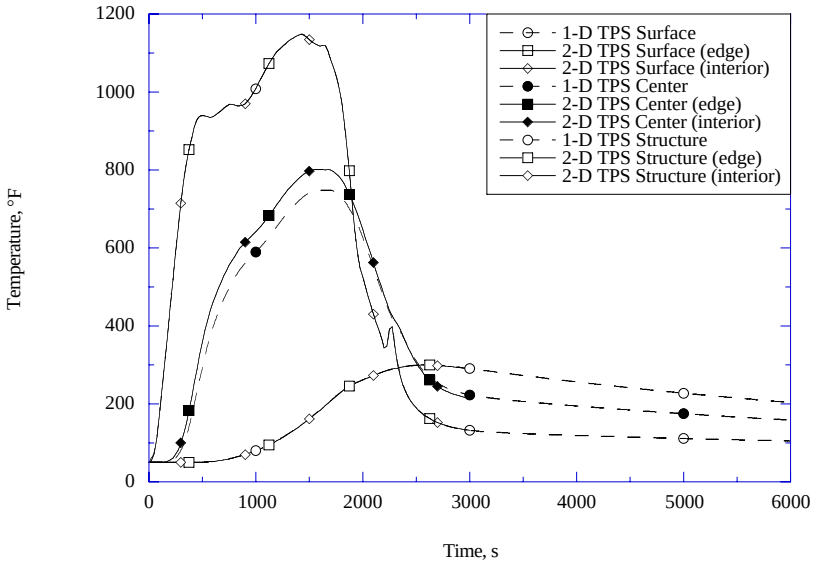

Figure 31. Transient thermal analysis results for the 1-D and 2-D AFRSI thermal models at Body Point B on RLV.

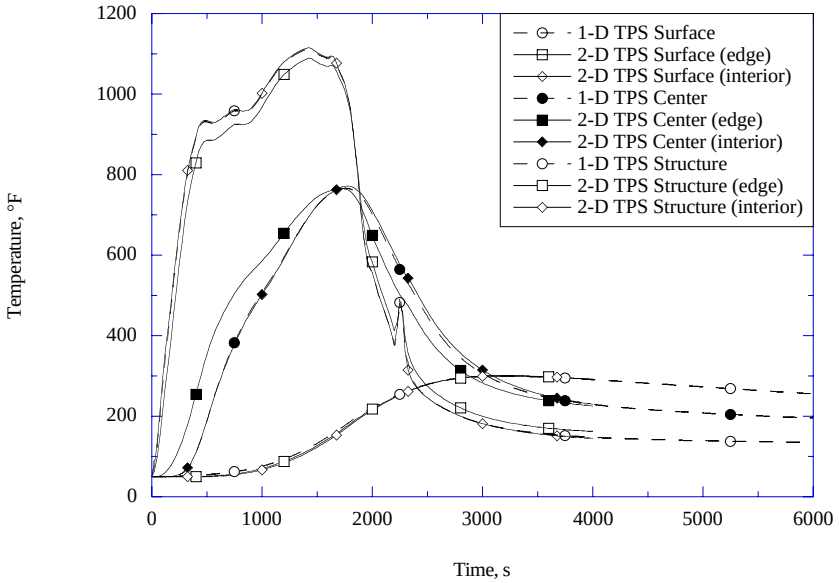

Figure 32. Transient thermal analysis results for the 1-D and 2-D TIMW thermal models at Body Point B on RLV.

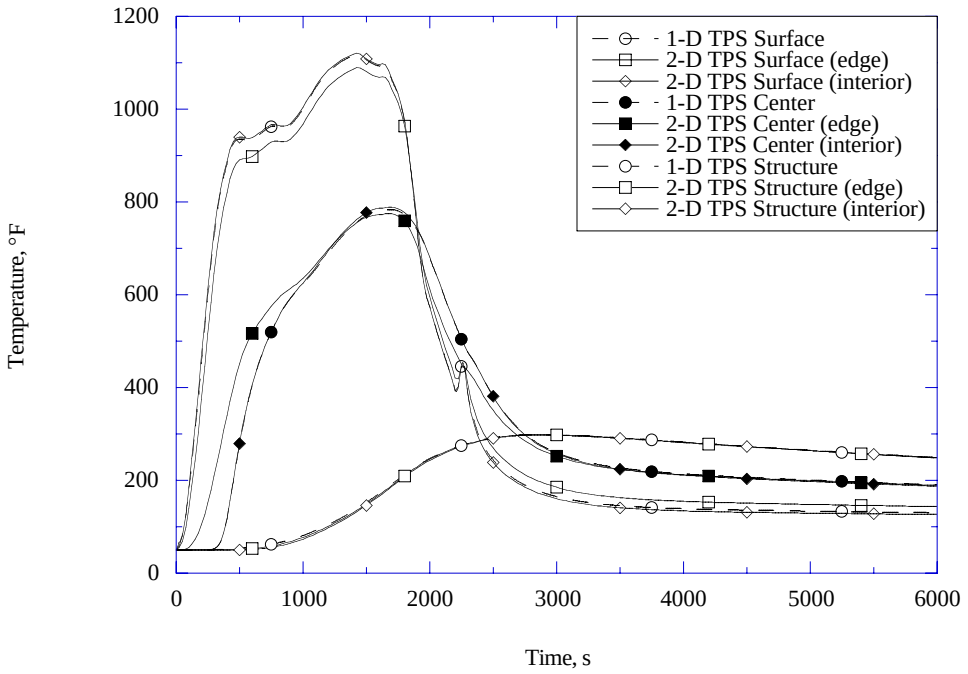

Figure 33. Transient thermal analysis results for the 1-D and 2-D TI/HC thermal models at Body Point B on RLV.

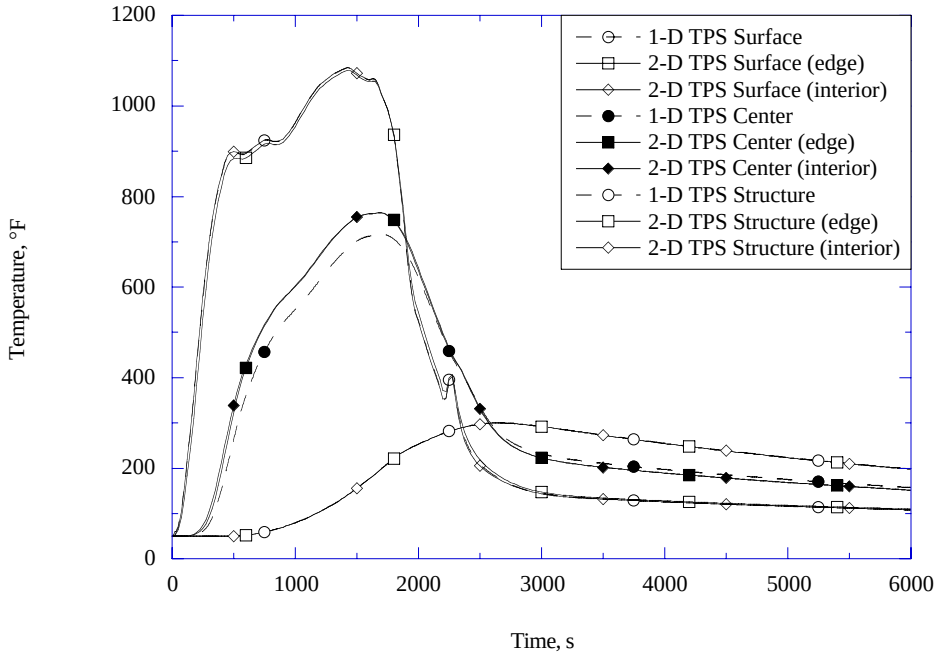

Figure 34. Transient thermal analysis results for the 1-D and 2-D TABI thermal models at Body Point B on RLV.

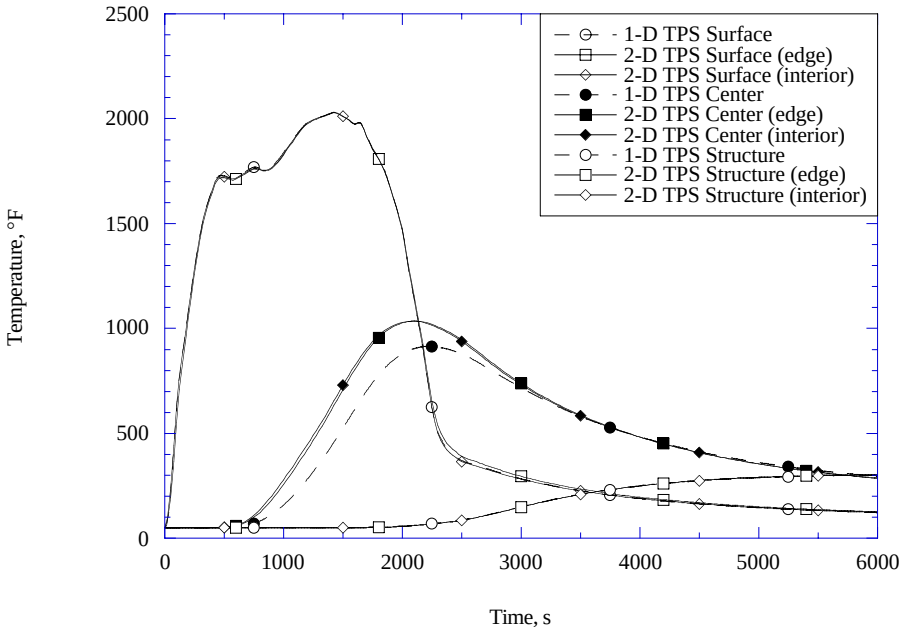

Figure 35. Transient thermal analysis results for the 1-D and 2-D TABI thermal models at Body Point A on RLV.

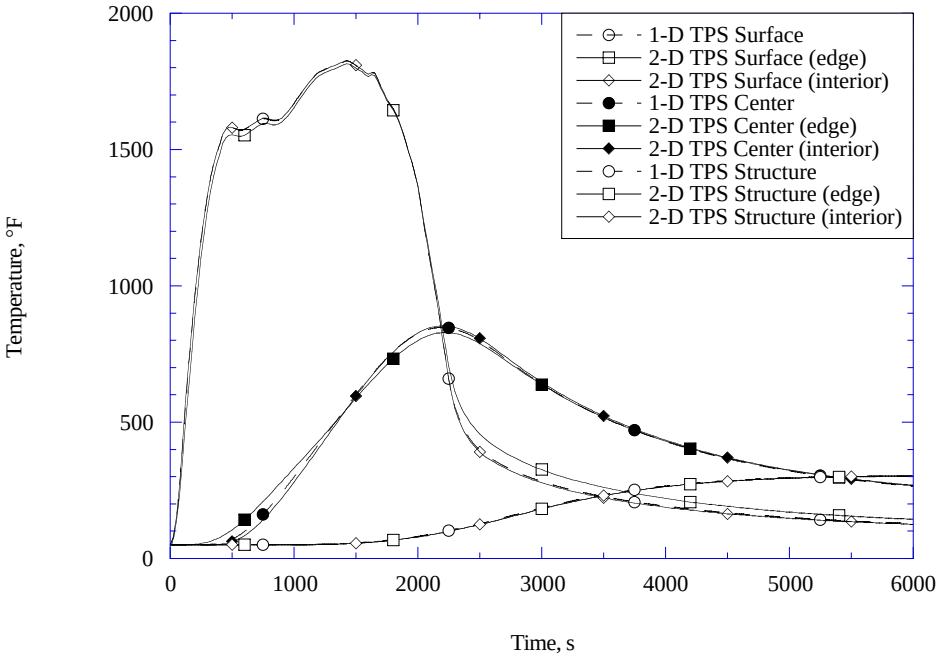

Figure 36. Transient thermal analysis results for the 1-D and 2-D AETB-8 thermal models at Body Point A on RLV.

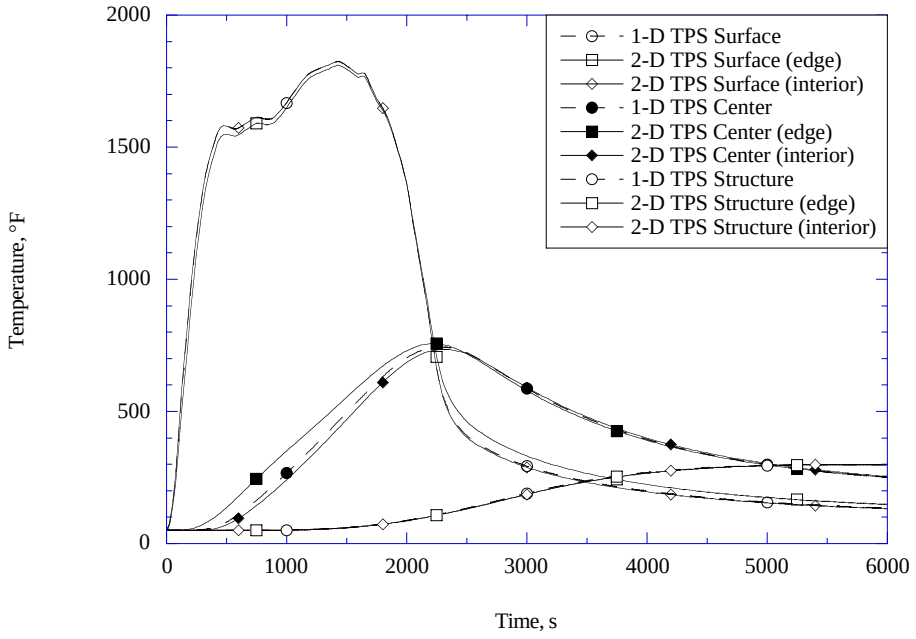

Figure 37. Transient thermal analysis results for the 1-D and 2-D AETB-12 thermal models at Body Point A on RLV.

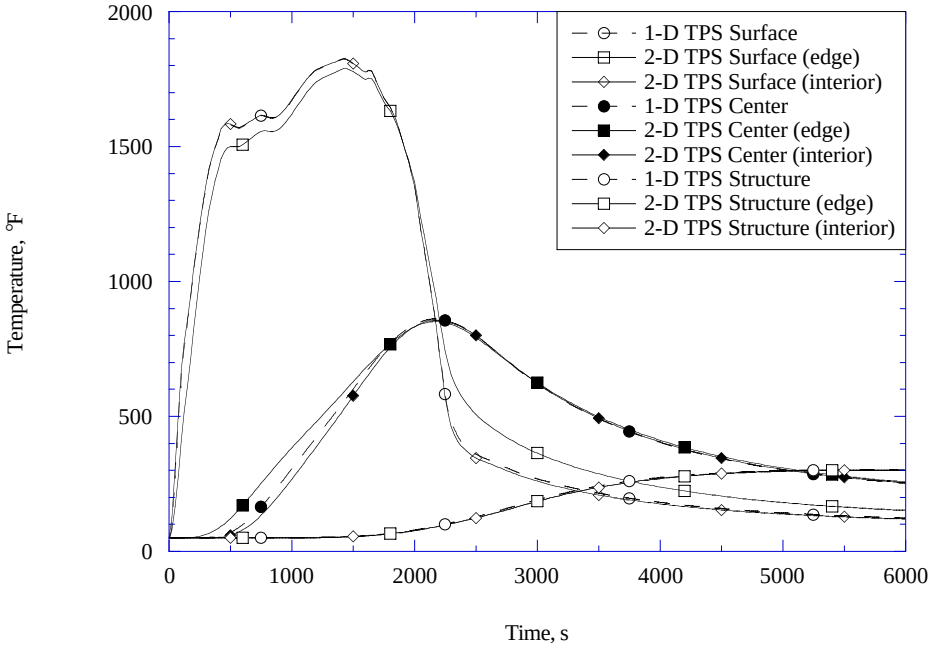

Figure 38. Transient thermal analysis results for the 1-D and 2-D LI-900 thermal models at Body Point A on RLV.

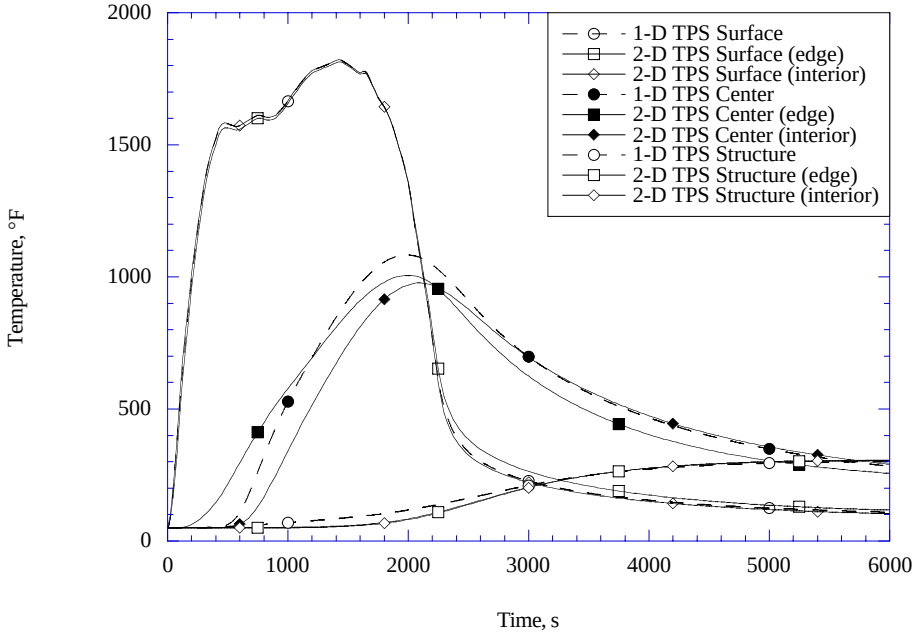

Figure 39. Transient thermal analysis results for the 1-D and 2-D SA/HC thermal models at Body Point A on RLV.

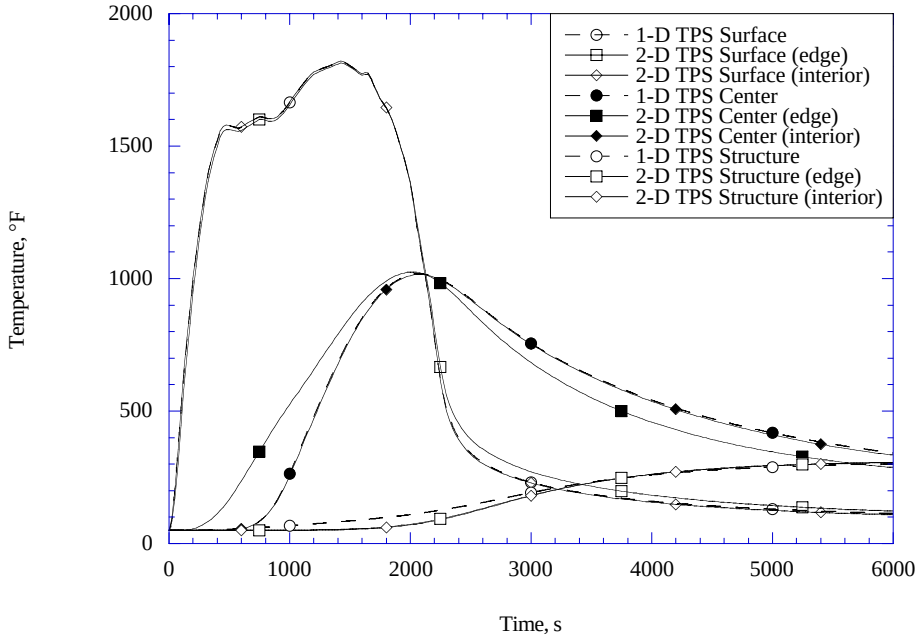

Figure 40. Transient thermal analysis results for the 1-D and 2-D SA/HC2 thermal models at Body Point A on RLV.

APPENDIX C

Material Properties Used in the Thermal Models

Table 4. List of material property tables used in the thermal models.

Table Number	Material Property
5	RTV Specific Heat
6	RTV Conductivity
7	AB312 Specific Heat
8	AB312 Conductivity
9	TABI Specific Heat
10	TABI Conductivity
11	TABI Emissivity
12	AFRSI Specific Heat
13	AFRSI Conductivity
14	C9 Coating Specific Heat
15	C9 Coating Emissivity
16	LI-900 Specific Heat
17	LI-900 Conductivity
18	Nomex Felt-RTV Coated Conductivity
19	LI-900 RCG Coated Specific Heat
20	LI-900 RCG Coated Conductivity
21	AETB-8 Specific Heat
22	AETB-8 Conductivity
23	TUFI Specific Heat
24	TUFI Conductivity
25	AETB-12 Specific Heat
26	AETB-12 Conductivity
27	Aluminum Specific Heat
28	Titanium 6-4 Specific Heat
29	Titanium 6-4 Conductivity
30	Titanium 6-2-4-2 Honeycomb Conductivity
31	TIMW Conductivity
32	Inconel 617 Specific Heat
33	Inconel 617 Conductivity
34	Inconel 617 Honeycomb Conductivity
35	PM2000 Specific Heat
36	PM2000 Conductivity
37	Saffil Specific Heat
38	Saffil Conductivity
39	Q-Fiber Felt Specific Heat
40	Q-Fiber Felt Conductivity
41	Cerrachrome Specific Heat
42	Cerrachrome Conductivity
43	IMI Specific Heat
44	IMI Conductivity

RTV Adhesive[18]
density: 88 lb/ft^3

Table 5. Specific Heat, c_p (Btu/lb-°R) vs. Temperature (°R) for RTV

T	320	360	410	460	560	660	860	1000
c_p	0.273	0.270	0.260	0.265	0.285	0.300	0.340	0.340

Table 6. Conductivity, k (Btu/ft-s-°R) vs. Temperature (°R) for RTV

T	260	360	460	660	860	960
k	6.47E-5	6.94E-5	6.81E-5	5.56E-5	4.53E-5	4.06E-5

AB312[18]
density: 61.5 lb/ft^3

Table 7. Specific Heat, c_p (Btu/lb-°R) vs. Temperature (°R) for AB312

T	860	960	1060	1160	1260	1460	1660	1860	2060	2260	2460	2660
c_p	0.202	0.214	0.223	0.230	0.236	0.244	0.251	0.256	0.261	0.266	0.270	0.275

Table 8. Conductivity, k (Btu/ft-s-°R) vs. Temperature (°R) for AB312

T	660	860	1060	1260	1460	1660	1860	2060	2260	2460
k	1.00E-5	1.22E-5	1.47E-5	1.72E-5	1.97E-5	2.31E-5	2.69E-5	3.17E-5	3.75E-5	4.39E-5

TABI[18]
density: 6 lb/ft^3 (batting material)

Table 9. Specific Heat, c_p (Btu/lb-°R) vs. Temperature (°R) for TABI batting

T	210	310	460	710	960	1210	1460	1710	1960	2160	2260
c_p	0.070	0.105	0.150	0.210	0.252	0.275	0.288	0.296	0.300	0.302	0.303

Table 10. Conductivity, k (Btu/ft-s-°R) vs. Temperature (°R) and Pressure (lb/ft^2) for TABI batting (Q-Felt)

	Pressure					
Temperature	0.001	0.2784	2.784	27.84	278.4	2116
260	7.50E-7	7.50E-7	1.17E-6	2.17E-6	3.44E-6	3.89E-6
460	1.44E-6	1.44E-6	2.17E-6	3.89E-6	6.17E-6	6.89E-6
560	1.83E-6	1.83E-6	2.75E-6	4.78E-6	7.56E-6	8.50E-6
760	2.64E-6	2.64E-6	3.86E-6	6.58E-6	1.04E-5	1.16E-5
960	3.67E-6	3.67E-6	5.14E-6	8.53E-6	1.32E-5	1.49E-5

Table 10. Continued

1160	5.03E-6	5.03E-6	6.58E-6	1.06E-5	1.63E-5	1.83E-5
1360	6.72E-6	6.72E-6	8.50E-6	1.29E-5	1.94E-5	2.20E-5
1610	9.56E-6	9.56E-6	1.16E-5	1.65E-5	2.39E-5	2.67E-5
1760	1.15E-5	1.15E-5	1.41E-5	1.92E-5	2.67E-5	3.00E-5
1960	1.48E-5	1.48E-5	1.77E-5	2.28E-5	3.06E-5	3.44E-5
2260	2.10E-5	2.10E-5	2.67E-5	3.11E-5	4.11E-5	4.33E-5

Table 11. Emissivity, ε vs. Temperature (°R) used for C9 Coating on TABI[15]

T	460	710	960	1210	1460	1710	1960	2210	2460
ε	0.87	0.84	0.80	0.77	0.74	0.70	0.67	0.64	0.60

AFRSI[15]

density: 6 lb/ft^3 (batting material)

Table 12. Specific Heat, c_p (Btu/lb-°R) vs. Temperature (°R) for AFRSI batting

T	460	710	960	1210	1460	1710	1960	2210	2460
c_p	0.177	0.212	0.244	0.270	0.277	0.269	0.282	0.295	0.307

Table 13. Conductivity, k (Btu/ft-s-°R) vs. Temperature (°R) and Pressure (lb/ft^2) for AFRSI batting (Q-fiber felt)

	Pressure				
Temperature	0.2126	2.126	21.16	211.6	2116.
460	1.11E-6	1.67E-6	4.17E-6	4.72E-6	5.28E-6
710	1.94E-6	2.78E-6	5.83E-6	7.22E-6	8.33E-6
960	2.78E-6	3.89E-6	7.22E-6	1.00E-5	1.14E-6
1210	4.17E-6	5.28E-6	8.89E-6	1.28E-5	1.47E-6
1460	5.83E-6	7.22E-6	1.11E-5	1.58E-5	1.83E-5
1710	8.33E-6	1.00E-5	1.44E-5	1.94E-5	2.22E-5
1960	1.11E-5	1.33E-5	1.83E-5	2.33E-5	2.64E-5
2210	1.50E-5	1.72E-5	2.22E-5	2.92E-5	3.33E-5

C9 Coating[15]

density: 125 lb/ft^3

Table 14. Specific Heat, c_p (Btu/lb-°R) vs. Temperature (°R) for C9

T	460	710	960	1210	1460	1710	1960	2110	2460
c_p	0.177	0.212	0.244	0.270	0.277	0.269	0.282	0.295	0.307

Table 15. Emissivity, ε vs. Temperature (°R) for C9 Coating on AFRSI

T	460	710	960	1210	1460	1710	1960	2210	2460
ε	0.87	0.84	0.81	0.71	0.66	0.59	0.54	0.47	0.45

LI-900[18]
density: 9 lb/ft^3

Table 16. Specific Heat, c_p (Btu/lb-°R) vs. Temperature (°R) for LI-900

T	210	310	460	710	960	1210	1460	1710	1960	2160	2210	3460
c_p	0.070	0.105	0.150	0.210	0.252	0.275	0.288	0.296	0.300	0.302	0.303	0.303

Table 17. Conductivity, k (Btu/ft-s-°R) vs. Temperature (°R) and Pressure (lb/ft^2) for LI-900

	Pressure					
Temperature	0.001	0.2126	2.126	21.16	211.6	2116
210	1.39E-6	1.39E-6	2.08E-6	4.17E-6	6.00E-6	6.47E-6
460	2.08E-6	2.08E-6	2.78E-6	5.08E-6	6.94E-6	7.64E-6
710	2.56E-6	2.56E-6	3.47E-6	6.25E-6	8.78E-6	9.47E-6
960	3.47E-6	3.47E-6	4.64E-6	7.67E-6	1.11E-5	1.20E-5
1210	4.86E-6	4.86E-6	6.00E-6	9.03E-6	1.37E-5	1.48E-5
1460	6.47E-6	6.47E-6	7.64E-6	1.09E-5	1.67E-5	1.83E-5
1710	8.56E-6	8.56E-6	9.72E-6	1.37E-5	2.01E-5	2.17E-5
1960	1.16E-5	1.16E-5	1.28E-5	1.71E-5	2.43E-5	2.62E-5
2210	1.58E-5	1.58E-5	1.69E-5	2.13E-5	2.94E-5	3.13E-5
2460	2.04E-5	2.04E-5	2.17E-5	2.62E-5	3.53E-5	3.75E-5
2760	2.68E-5	2.68E-5	2.83E-5	3.22E-5	4.31E-5	4.64E-5
2960	3.22E-5	3.22E-5	3.42E-5	3.86E-5	4.97E-5	5.39E-5
3260	4.27E-5	4.27E-5	4.50E-5	5.00E-5	6.17E-5	6.72E-5
3460	5.28E-5	5.28E-5	5.44E-5	6.08E-5	7.28E-5	8.06E-5

Nomex Felt - RTV Coated[22]
density: 12.27 lb/ft^3
specific heat: 0.29 Btu/lb-°R

Table 18. Conductivity, k (Btu/ft-s-°R) vs. Temperature (°R) for Nomex Felt

T	460	860	1060	2470
k	5.25E-6	7.44E-6	1.06E-5	2.12E-5

LI-900 RCG Coating[18]
density: 104 lb/ft^3
emissivity: 0.85

Table 19. Specific Heat, c_p (Btu/lb-°R) vs. Temperature (°R) for LI-900 Coating

T	530	960	1460	1960	2460
c_p	0.190	0.240	0.280	0.320	0.340

Table 20. Conductivity, k (Btu/ft-s-°R) vs. Temperature (°R) for LI-900 RCG Coating

T	530	960	1460	1960	2460
k	1.39E-4	1.71E-4	1.85E-4	2.53E-4	2.92E-4

AETB-8[17]
density: 8 lb/ft^3

Table 21. Specific Heat, c_p (Btu/lb-°R) vs. Temperature (°R) for AETB-8

T	460	710	960	1210	1460	1710	1960	2210	3210
c_p	0.150	0.210	0.252	0.275	0.288	0.296	0.300	0.303	0.303

Table 22. Conductivity, k (Btu/ft-s-°R) vs. Temperature (°R) and Pressure (lb/ft^2) for AETB-8

	Pressure					
Temperature	0.001	0.2116	2.116	21.16	211.6	2116.
460	2.78E-6	2.78E-6	4.17E-6	7.22E-6	8.33E-6	8.33E-6
710	3.06E-6	3.06E-6	4.44E-6	8.06E-6	9.72E-6	1.00E-5
960	4.17E-6	4.17E-6	5.56E-6	9.44E-6	1.19E-5	1.22E-5
1210	6.11E-6	6.11E-6	7.22E-6	1.17E-5	1.47E-5	1.53E-5
1460	8.61E-6	8.61E-6	9.44E-6	1.42E-5	1.67E-5	1.86E-5
1710	1.14E-5	1.14E-5	1.25E-5	1.72E-5	2.14E-5	2.22E-5
1960	1.50E-5	1.50E-5	1.58E-5	2.06E-5	2.56E-5	2.64E-5
2210	2.11E-5	2.11E-5	1.94E-5	2.42E-5	2.97E-5	3.08E-5
2460	2.25E-5	2.25E-5	2.33E-5	2.83E-5	3.42E-5	3.56E-5
2710	2.67E-5	2.67E-5	2.75E-5	3.22E-5	3.86E-5	4.03E-5
2960	3.06E-5	3.06E-5	3.14E-5	3.67E-5	4.31E-5	4.47E-5
3210	3.17E-5	3.17E-5	3.25E-5	3.69E-5	4.36E-5	4.56E-5

TUFI COATING[15]
density: 50 lb/ft^3
emissivity: 0.85

Table 23. Specific Heat, c_p (Btu/lb-°R) vs. Temperature (°R) for TUFI

T	460	660	860	1060	1260	1460	1660	1860	2060	2260	2460	2660	2860	3060
c_p	0.220	0.229	0.235	0.241	0.244	0.249	0.253	0.258	0.265	0.271	0.278	0.285	0.291	0.296

Table 24. Conductivity, k (Btu/ft-s-°R) vs. Temperature (°R) for TUFI

T	460	660	860	1060	1260	1460	1660
k	1.28E-4	1.08E-4	9.86E-5	9.39E-5	9.22E-5	9.22E-5	9.39E-5
T	1860	2060	2260	2460	2660	2860	3060
k	9.72E-5	1.02E-4	1.08E-4	1.15E-4	1.24E-4	1.34E-4	1.46E-4

AETB-12[17]
density: 12 lb/ft^3

Table 25. Specific Heat, c_p (Btu/lb-°R) vs. Temperature (°R) for AETB-12

T	460	710	960	1210	1460	1710	1960	2210	3210
c_p	0.150	0.210	0.252	0.275	0.288	0.296	0.300	0.303	0.303

Table 26. Conductivity, k (Btu/ft-s-°R) vs. Temperature (°R) and Pressure (lb/ft^2) for AETB-12

	Pressure					
Temperature	0.001	0.2116	2.116	21.16	211.6	2116.
460	4.72E-6	4.72E-5	5.83E-6	8.89E-6	1.03E-5	1.03E-5
710	4.17E-6	4.17E-6	5.28E-6	8.89E-6	1.08E-5	1.11E-5
960	4.44E-6	4.44E-6	5.28E-6	9.17E-6	1.19E-5	1.22E-5
1210	5.00E-6	5.00E-6	5.83E-6	1.00E-5	1.33E-5	1.39E-5
1460	6.11E-6	6.11E-6	6.94E-6	1.08E-5	1.50E-5	1.58E-5
1710	7.22E-6	7.22E-6	8.06E-6	1.22E-5	1.69E-5	1.78E-5
1960	8.89E-6	8.89E-6	9.44E-6	1.36E-5	1.89E-5	2.00E-5
2210	1.06E-5	1.06E-5	1.11E-5	1.56E-5	2.11E-5	2.25E-5
2460	1.22E-5	1.22E-5	1.31E-5	1.69E-5	2.33E-5	2.50E-5
2710	1.42E-5	1.42E-5	1.47E-5	1.89E-5	2.56E-5	2.72E-5
2960	1.58E-5	1.58E-5	1.64E-5	2.07E-5	2.75E-5	2.97E-5
3210	1.64E-5	1.64E-5	1.69E-5	2.06E-5	2.75E-5	2.97E-5

Aluminum[18]
density: 175 lb/ft^3

Table 27. Specific heat, c_p (Btu/lb-°R) vs. Temperature (°R) for Aluminum

T	160	460	660	760	860
c_p	0.177	0.195	0.216	0.224	0.233

Titanium 6-4[18]
density: 277 lb/ft^3
emissivity: 0.6

Table 28. Specific Heat, c_p (Btu/lb-°R) vs. Temperature (°R) for Titanium

T	60	260	460	660	860	1060	1260	1460	1660	1860	2060
c_p	0.012	0.096	0.125	0.136	0.138	0.144	0.153	0.167	0.182	0.205	0.225

Table 29. Conductivity, k (Btu/ft-s-°R) vs. Temperature (°R) for Titanium 6-4

T	60	260	460	660	860	1060	1260	1460	1660	1860	2060
k	3.33E-4	9.44E-4	1.11E-3	1.19E-3	1.39E-3	1.67E-3	1.92E-3	2.19E-3	2.39E-3	2.67E-3	2.89E-3

Titanium 6-2-4-2 Honeycomb[22]

Table 30. Conductivity, k (Btu/ft-s-°R) vs. Temperature (°R) for Titanium Honeycomb

T	0	460	560	660	860	1060	1260	1460	1960	2460
k	1.11E-5	1.81E-5	2.11E-5	2.44E-5	3.14E-5	3.92E-5	4.86E-5	5.97E-5	7.81E-5	9.89E-5

Titanium Multiwall (TIMW)[23]

density : 13.2 lb/ft^3

Table 31. Conductivity, k (Btu/ft-s-°R) vs. Temperature (°R) and Pressure (lb/ft^2) for Titanium Multiwall (data for reduced pressures predicted using air conductivity data)

	Pressure						
Temperature	0.0278	0.278	2.785	27.85	139.2	278.4	2116.
460	2.44E-6	2.72E-6	4.25E-6	6.19E-6	6.56E-6	6.61E-6	6.67E-6
710	4.28E-6	4.53E-6	6.14E-6	8.67E-6	9.28E-6	9.39E-6	9.44E-6
960	6.19E-6	6.42E-6	8.03E-6	1.14E-5	1.25E-5	1.26E-5	1.28E-5
1060	7.31E-6	7.50E-6	9.11E-6	1.28E-5	1.41E-5	1.43E-5	1.44E-5
1160	8.75E-6	8.94E-6	1.05E-5	1.45E-5	1.59E-5	1.62E-5	1.64E-5
1260	1.05E-5	1.07E-5	1.22E-5	1.65E-5	1.81E-5	1.84E-5	1.86E-5
1360	1.25E-5	1.27E-5	1.42E-5	1.87E-5	2.05E-5	2.08E-5	2.11E-5
1460	1.59E-5	1.61E-5	1.76E-5	2.23E-5	2.43E-5	2.47E-5	2.50E-5
1510	2.13E-5	2.14E-5	2.29E-5	2.77E-5	2.98E-5	3.02E-5	3.06E-5

Inconel 617[22]

density: 521 lb/ft^3

emissivity: 0.86

Table 32. Specific Heat, c_p (Btu/lb-°R) vs. Temperature (°R) for Inconel 617

T	538	660	860	1060	1260	1460	1660	1860	2060	2460
c_p	0.100	0.104	0.111	0.117	0.124	0.131	0.137	0.144	0.150	0.163

Table 33. Conductivity, k (Btu/ft-s-°R) vs. Temperature (°R) for Inconel 617

T	538	660	860	1060	1260	1460	1660	1860	2060	2260	2460
k	2.18E-3	2.34E-3	2.62E-3	2.89E-3	3.17E-3	3.45E-3	3.73E-3	4.00E-3	4.28E-3	4.56E-3	4.84E-3

Table 34. Conductivity, k (Btu/ft-s-°R) vs. Temperature (°R) for Inconel 617 Honeycomb

T	560	660	860	1060	1260	1460	1660	1860	2060	2260	2460
k	4.11E-5	4.64E-5	5.67E-5	6.97E-5	8.64E-5	1.07E-4	1.32E-4	1.63E-4	2.00E-4	2.43E-4	2.93E-4

PM2000[24]
density: 449.28 lb/ft^3
The following data is for MA956 which is chemically similar to PM2000.
emissivity: 0.70

Table 35. Specific heat, c_p (Btu/lb-°R) vs. Temperature (°R) for PM2000

T	460	860	1260	1660	2060	2460
cp	0.108	0.123	0.138	0.153	0.168	0.184

Table 36. Conductivity, K (Btu/ft-s-°R) vs. Temperature (°R) for PM2000

T	460	860	1260	1660	2060	2460	2560
k	1.69E-3	2.22E-3	2.69E-3	3.25E-3	3.81E-3	4.31E-3	4.44E-3

Conductivity data for PM2000 Honeycomb was unavailable. IN617 Honeycomb (table 30) was used.

Saffil (used in Second Generation Superalloy Honeycomb Metallic TPS)[23]
density: 3.12 lb/ft^3

Table 37. Specific heat, c_p (Btu/lb-°R) vs. Temperature (°R) for Advanced Saffil

T	460	700	900	1100	1300	1500	1700	2100
c_p	0.225	0.225	0.248	0.274	0.292	0.302	0.312	0.320

Table 38. Conductivity, k (Btu/ft-s-°R) vs. Temperature (°R) and Pressure (lb/ft^2) (data for reduced pressures predicted using air conductivity data)

	Pressure						
Temperature	0.0278	0.2785	2.785	27.85	139.20	278.4	2116.
660	8.61E-7	1.11E-6	2.69E-6	5.06E-6	5.58E-6	5.67E-6	5.72E-6
860	2.28E-6	2.53E-6	4.14E-6	7.22E-6	8.08E-6	8.22E-6	8.33E-6
1060	4.36E-6	4.56E-6	6.17E-6	9.89E-6	1.11E-5	1.13E-5	1.15E-5
1260	7.72E-6	7.92E-6	9.47E-6	1.37E-5	1.53E-5	1.56E-5	1.59E-5
1460	1.24E-5	1.25E-5	1.41E-5	1.87E-5	2.07E-5	2.11E-5	2.14E-5
1660	1.48E-5	1.50E-5	1.64E-5	2.14E-5	2.39E-5	2.43E-5	2.48E-5
1860	2.47E-5	2.50E-5	2.64E-5	3.17E-5	3.46E-5	3.52E-5	3.57E-5
2060	3.30E-5	3.34E-5	3.49E-5	4.08E-5	4.41E-5	4.47E-5	4.53E-5
2260	4.25E-5	4.29E-5	4.45E-5	5.08E-5	5.43E-5	5.49E-5	5.56E-5
2460	5.46E-5	5.50E-5	5.68E-5	6.38E-5	6.76E-5	6.84E-5	7.18E-5
2660	7.22E-5	7.26E-5	7.45E-5	8.18E-5	8.58E-5	8.66E-5	8.73E-5
2860	9.18E-5	9.23E-5	9.43E-5	1.02E-4	1.06E-4	1.07E-4	1.08E-4
3060	1.14E-4	1.14E-4	1.16E-4	1.25E-4	1.29E-4	1.30E-4	1.31E-4
3260	1.45E-4	1.45E-4	1.47E-4	1.56E-4	1.61E-4	1.62E-4	1.63E-4
3460	1.79E-4	1.80E-4	1.82E-4	1.91E-4	1.97E-4	1.98E-4	1.98E-4

Q-Fiber Felt[22]

density: 3.5 lb/ft^3 (batting material - metallic concepts).

Table 39. Specific heat, c_p (Btu/lb-°R) vs. Temperature (°R) for Q-fiber

T	700	900	790	1300	1500	1700	2100
c_p	0.202	0.233	0.252	0.267	0.274	0.280	0.284

Table 40. Conductivity, k (Btu/ft-s-°R) vs. Temperature (°R) and Pressure (lb/ft^2) for Q-fiber

	Pressure						
Temperature	0.0278	0.278	2.785	27.85	139.2	278.4	2116.
560	8.33E-7	8.33E-7	2.36E-6	4.31E-6	4.67E-6	4.72E-6	4.78E-6
660	1.39E-6	1.64E-6	3.22E-6	5.58E-6	6.11E-6	6.19E-6	6.25E-6
760	2.17E-6	2.42E-6	4.03E-6	6.78E-6	7.44E-6	7.56E-6	7.64E-6
860	2.97E-6	3.22E-6	4.83E-6	7.92E-6	8.78E-6	8.92E-6	9.03E-6
1060	5.03E-6	5.22E-6	6.83E-6	1.06E-5	1.18E-5	1.20E-5	1.22E-5
1260	7.42E-6	7.61E-6	9.17E-6	1.34E-5	1.50E-5	1.88E-5	1.56E-5
1460	1.01E-5	1.03E-5	1.18E-5	1.64E-5	1.85E-5	1.88E-5	1.92E-5
1660	1.32E-5	1.34E-5	1.48E-5	1.98E-5	2.23E-5	2.27E-5	2.31E-5
1860	1.58E-5	1.61E-5	1.78E-5	2.39E-5	2.67E-5	2.72E-5	2.78E-5
1960	1.72E-5	1.75E-5	1.94E-5	2.58E-5	2.92E-5	2.97E-5	3.03E-5
2060	1.92E-5	1.94E-5	2.14E-5	2.86E-5	3.22E-5	3.28E-5	3.33E-5
2260	2.22E-5	2.25E-5	2.50E-5	3.33E-5	3.75E-5	3.53E-5	3.89E-5

Cerrachrome Insulation[22]

density: 6.0 lb/ft^3

Table 41. Specific Heat, c_p (Btu/lb-°R) vs. Temperature (°R) for Cerrachrome

T	460	660	860	1060	1260	1460	1660	1860	2060	2260	2460	2660	2860
c_p	0.165	0.196	0.227	0.248	0.264	0.273	0.279	0.281	0.284	0.287	0.290	0.293	0.297

Table 42. Conductivity, k (Btu/ft-s-°R) vs. Temperature (°R) and Pressure (lb/ft^2) for Cerrachrome

	Pressure						
Temperature	0.0278	0.278	2.78	27.8	139.	278.	2116.
660.	.119E-5	.133E-5	.244E-5	.494E-5	.572E-5	.586E-5	.597E-5
860.	.294E-5	.308E-5	.417E-5	.725E-5	.850E-5	.869E-5	.889E-5
1060.	.481E-5	.492E-5	.594E-5	.950E-5	.112E-4	.115E-4	.118E-4
1260.	.708E-5	.719E-5	.817E-5	.120E-4	.142E-4	.146E-4	.151E-4
1460.	.102E-4	.104E-4	.113E-4	.154E-4	.180E-4	.186E-4	.191E-4
1660.	.147E-4	.148E-4	.157E-4	.199E-4	.231E-4	.237E-4	.244E-4
1860.	.196E-4	.197E-4	.206E-4	.249E-4	.284E-4	.292E-4	.301E-4
2060.	.258E-4	.259E-4	.267E-4	.311E-4	.351E-4	.360E-4	.370E-4
2260.	.321E-4	.322E-4	.330E-4	.374E-4	.417E-4	.428E-4	.440E-4

Table 42. Continued

2460.	.407E-4	.408E-4	.416E-4	.459E-4	.506E-4	.519E-4	.532E-4
2660.	.507E-4	.508E-4	.515E-4	.559E-4	.609E-4	.623E-4	.639E-4
2860.	.604E-4	.604E-4	.611E-4	.655E-4	.708E-4	.724E-4	.742E-4

IMI Insulation

density: 4.554 lb/ft^3

Table 43. Specific heat, c_p (Btu/lb-°R) vs. Temperature (°R) for IMI

T	460	660	860	1060	1260	1460	1660	1860	2060	2260	2460
c_p	0.157	0.200	0.224	0.237	0.244	0.250	0.255	0.259	0.264	0.268	0.268

Table 44. Conductivity, k (Btu/ft-s-°R) vs. Temperature (°R) and Pressure (lb/ft^2) for IMI (data predicted using analytical methods)

	Pressure						
Temperature	0.00278	0.02780	0.2785	2.784	27.84	278.4	2116.
460	1.01E-6	1.03E-6	1.14E-6	1.99E-6	4.06E-6	4.86E-6	4.97E-6
660	1.06E-6	1.07E-6	1.16E-6	1.88E-6	4.28E-6	5.61E-6	5.81E-6
860	1.21E-6	1.21E-6	1.29E-6	1.97E-6	4.72E-6	6.72E-6	7.06E-6
1060	1.66E-6	1.67E-6	1.74E-6	2.38E-6	5.39E-6	8.03E-6	8.53E-6
1260	2.46E-6	2.47E-6	2.54E-6	3.17E-6	6.33E-6	9.61E-6	1.03E-5
1460	3.67E-6	3.67E-6	3.72E-6	4.33E-6	7.61E-6	1.15E-5	1.24E-5
1660	5.33E-6	5.33E-6	5.39E-6	5.94E-6	9.28E-6	1.37E-5	1.48E-5
1860	7.58E-6	7.61E-6	7.67E-6	8.19E-6	1.16E-5	1.65E-5	1.78E-5
2060	1.08E-5	1.08E-6	1.08E-5	1.14E-5	1.48E-5	2.02E-5	2.17E-5
2260	1.48E-5	1.48E-6	1.49E-5	1.54E-5	1.88E-5	2.48E-5	2.65E-5
2460	1.96E-5	1.96E-5	1.97E-5	2.01E-5	2.34E-5	2.94E-5	3.14E-5
2660	2.54E-5	2.54E-5	2.55E-5	2.59E-5	2.89E-5	3.53E-5	3.72E-5
2860	3.17E-5	3.17E-5	3.17E-5	3.22E-5	3.50E-5	4.14E-5	4.36E-5

APPENDIX D

Component Weight Models for the Various TPS Concepts

In this section, the weight equations for each TPS system are determined and shown. The 1-D code calculated a converged insulation thickness for each system and used the value in the corresponding weight equation to determine the total TPS weight.

Table 45. Weight Calculations for AFRSI

Item	Thickness (in.)	Density (lb/ft^3)	Unit Weight (lb/ft^2)
Protective Coating	0.010	125.0	0.104
Outer Fabric	0.011	61.5	0.056
Insulation	t	6.0	0.50t
Inner Fabric	0.009	61.5	0.046
RTV Adhesive	0.008	88.0	0.059
Edge Closeout	.011	61.5	.007t

AFRSI Weight = 0.265 + 0.507t

Table 46. Weight Calculations for TABI

Item	Thickness (in.)	Density (lb/ft^3)	Unit Weight (lb/ft^2)
Protective Coating	0.010	125.	0.108
Outer Fabric	0.011	55	0.056
Insulation	t	6.0	0.50t
Corrugation	0.009*2	55	0.092
Inner Fabric	0.009	55	0.046
RTV Adhesive	0.008	88.0	0.055
Edge Closeout	.011	61.5	.007t

TABI Weight = 0.357 + 0.507t

Table 47. Weight Calculations for LI-900

Item	Thickness (in.)	Density (lb/ft^3)	Unit Weight (lb/ft^2)
Protective Coating (top)	0.012	104.0	0.104
Protective Coating (side)	0.012	104.0	0.0693t
LI-900	t	9.0	0.750t
Densified Region	0.010	24.0	0.20
RTV Adhesive	0.008*2	88.0	0.117
Nomex SIP	0.160	5.4	0.072

LI-900 Weight = 0.493 + 0.819t

Table 48. Weight Calculations for AETB-8

Item	Thickness (in.)	Density (lb/ft^3)	Unit Weight (lb/ft^2)
Protective Coating (top)	0.100	50.0	0.417
Protective Coating (side)	0.020	50.0	0.042t
AETB-8	t	8.0	0.667t
RTV Adhesive	0.008*2	88.0	0.117
Nomex SIP	0.160	5.4	0.072

AETB-8 Weight = 0.606 + 0.709t

Table 49. Weight Calculations for AETB-12

Item	Thickness (in.)	Density (lb/ft^3)	Unit Weight (lb/ft^2)
Protective Coating (top)	0.100	50.0	0.417
Protective Coating (side)	0.020	50.0	0.042t
AETB-12	t	12.0	t
RTV Adhesive	0.008*2	88.0	0.117
Nomex SIP	0.160	5.4	0.072

AETB-12 Weight = 0.606 + 1.042t

Table 50. Weight Calculations for Titanium Multiwall (TIMW)

Item	Thickness (in.)	Density (lb/ft^3)	Unit Weight (lb/ft^2)
Titanium Sidewall	0.003	283.	0.024(t+0.2)
Titanium Multiwall	t	9.0	0.750t
RTV/Nomex Felt	0.190	12.3	0.031
Fasteners	n/a	n/a	0.061+.006t

TIMW Weight = 0.097 + 0.780t

Table 51. Weight Calculations for Super Alloy Honeycomb TPS (SA/HC)

Item	Thickness (in.)	Density (lb/ft^3)	Unit Weight (lb/ft^2)
IN617 Upper Facesheets	0.005*2	521.	0.456
Upper h/c core (IN617)	0.28	8.3	0.194
Q-Fiber	tx1	3.5	0.292tx1
Cerrachrome	tx2	6.0	0.50tx2
IN617 Sidewall	.003	521.	0.043(tx1+tx2+0.89)
Ti Lower Facesheets	.006/.003	277.	0.212
Lower h/c core (Ti)	0.17	5.9	0.083
Fasteners	n/a	n/a	0.087+0.011(tx1+tx2)
RTV/Nomex Felt	0.19	12.3	0.031
Braze Alloy	n/a	n/a	.095

SA/HC Weight = 1.196 + 0.346tx1 + 0.554tx2

Table: 52. Weight Calculations for Second Generation Super Alloy Honeycomb TPS (SA/HC2)

Item	Thickness (in.)	Density (lb/ft^3)	Unit Weight (lb/ft^2)
IN617 Upper Facesheets	0.005*2	521.	0.456
Upper h/c core (IN617)	0.28	8.3	0.194
Saffil	t	3.12	0.260t
In617 Sidewall	.003	521.	0.043(t+0.89)
Ti Lower Facesheets	.006/.003	277.	0.173
Lower h/c core (Ti)	0.17	5.9	0.036
Fasteners	n/a	n/a	0.087+0.011t
RTV/Nomex Felt	0.19	12.3	0.031
Braze Alloy	n/a	n/a	.085

SA/HC2 Weight =1.100 + 0.314t

Table 53. Weight Calculations for Titanium Honeycomb TPS (TI/HC)

Item	Thickness (in.)	Density (lb/ft^3)	Unit Weight (lb/ft^2)
Ti Upper Facesheets	0.005*2	277.	0.242
Upper h/c core (Ti)	0.28	5.9	0.138
Q-Fiber	t	3.5	0.292t
Ti Sidewall	.003	277.	0.023(t+0.89)
Ti Lower Facesheets	.006/.003	277.	0.173
Lower h/c core (Ti)	0.17	5.9	0.036
Fasteners	n/a	n/a	0.062+0.006t
RTV/Nomex Felt	0.19	12.3	0.031
Braze Alloy	n/a	n/a	.025

TIHC Weight = 0.727 + 0.321t

Table 54. Weight Calculations for Advanced Metallic Honeycomb TPS (AMHC)

Item	Thickness (in.)	Density (lb/ft^3)	Unit Weight (lb/ft^2)
PM2000 Upper Facesheets	0.005*2	449.	0.393
Upper h/c core (PM2000)	0.28	7.2	0.168
IMI Insulation	t	4.55	0.380t
PM2000 Sidewall	.003	521.	0.037(t+0.72)
Ti Lower Face	0.003	277.	0.073
Ti Tubular Frame	n/a	277.	0.121
Fasteners	n/a	n/a	0.028
RTV/Nomex Felt	0.19	12.3	0.031
Braze Alloy	n/a	n/a	0.078

PM2000 Weight =0.918 + 0.417t

REPORT DOCUMENTATION PAGE

Form Approved
OMB No. 0704-0188

Public reporting burden for this collection of information is estimated to average 1 hour per response, including the time for reviewing instructions, searching existing data sources, gathering and maintaining the data needed, and completing and reviewing the collection of information. Send comments regarding this burden estimate or any other aspect of this collection of information, including suggestions for reducing this burden, to Washington Headquarters Services, Directorate for Information Operations and Reports, 1215 Jefferson Davis Highway, Suite 1204, Arlington, VA 22202-4302, and to the Office of Management and Budget, Paperwork Reduction Project (0704-0188), Washington, DC 20503.

1. AGENCY USE ONLY (Leave blank)

2. REPORT DATE
June 2000

3. REPORT TYPE AND DATES COVERED
Technical Memorandum

4. TITLE AND SUBTITLE
Parametric Weight Comparison of Advanced Metallic, Ceramic Tile, and Ceramic Blanket Thermal Protection Systems

5. FUNDING NUMBERS
WU 242-33-01-50

6. AUTHOR(S)
David E. Myers, Carl J. Martin, and Max L. Blosser

7. PERFORMING ORGANIZATION NAME(S) AND ADDRESS(ES)
NASA Langley Research Center
Hampton, VA 23681-2199

8. PERFORMING ORGANIZATION REPORT NUMBER
L-17954

9. SPONSORING/MONITORING AGENCY NAME(S) AND ADDRESS(ES)
National Aeronautics and Space Administration
Washington, DC 20546-0001

10. SPONSORING/MONITORING AGENCY REPORT NUMBER
NASA/TM-2000-210289

11. SUPPLEMENTARY NOTES

12a. DISTRIBUTION/AVAILABILITY STATEMENT
Unclassified-Unlimited
Subject Category 15 Distribution: Standard
Availability: NASA CASI (301) 621-0390

12b. DISTRIBUTION CODE

13. ABSTRACT (Maximum 200 words)
A parametric weight assessment of advanced metallic panel, ceramic blanket, and ceramic tile thermal protection systems (TPS) was conducted using an implicit, one-dimensional (1-D) finite element sizing code. This sizing code contained models to account for coatings, fasteners, adhesives, and strain isolation pads. Atmospheric entry heating profiles for two vehicles, the Access to Space (ATS) vehicle and a proposed Reusable Launch Vehicle (RLV), were used to ensure that the trends were not unique to a certain trajectory. Ten TPS concepts were compared for a range of applied heat loads and substructural heat capacities to identify general trends. This study found the blanket TPS concepts have the lightest weights over the majority of their applicable ranges, and current technology ceramic tiles and metallic TPS concepts have similar weights. A proposed, state-of-the-art metallic system which uses a higher temperature alloy and efficient multilayer insulation was predicted to be significantly lighter than the ceramic tile systems and approaches blanket TPS weights for higher integrated heat loads.

14. SUBJECT TERMS
Thermal protection systems (TPS); Reusable launch vehicles (RLV); Thermal analysis

15. NUMBER OF PAGES
49

16. PRICE CODE
A03

17. SECURITY CLASSIFICATION OF REPORT
Unclassified

18. SECURITY CLASSIFICATION OF THIS PAGE
Unclassified

19. SECURITY CLASSIFICATION OF ABSTRACT
Unclassified

20. LIMITATION OF ABSTRACT
UL